the plant journal

SEB SOCIETY FOR EXPERIMENTAL BIOLOGY

The Plant Journal (2024) **119**, 960–981 doi: 10.1111/tpj.16809

A *Solanum lycopersicum* polyamine oxidase contributes to the control of plant growth, xylem differentiation, and drought stress tolerance

Riccardo D'Incà[1,†], Roberto Mattioli[1,†,‡], Martina Tomasella[2], Raffaela Tavazza[3], Alberto Macone[4], Alessio Incocciati[4], Damiano Martignago[5], Fabio Polticelli[1,6], Ilaria Fraudentali[1], Alessandra Cona[1,7], Riccardo Angelini[1,7,8], Mario Tavazza[3], Andrea Nardini[2] and Paraskevi Tavladoraki[1,7,*]

[1]*Department of Science, University Roma Tre, 00146 Rome, Italy,*
[2]*Dipartimento di Scienze della Vita, Università di Trieste, Trieste, Italy,*
[3]*Italian National Agency for New Technologies, Energy and Sustainable Economic Development (ENEA), BIOAG-BIOTEC C.R. Casaccia, Rome, Italy,*
[4]*Department of Biochemical Sciences 'A. Rossi Fanelli', Sapienza University of Rome, Rome, Italy,*
[5]*Department of Biosciences, University of Milano, Milan, Italy,*
[6]*National Institute of Nuclear Physics, Roma Tre Section, 00146 Rome, Italy,*
[7]*Istituto Nazionale Biostrutture e Biosistemi (INBB), Rome, Italy,*
[8]*NBFC, National Biodiversity Future Center, Palermo, Italy*

Received 2 November 2023; revised 26 April 2024; accepted 3 May 2024; published online 18 May 2024.
*For correspondence (e-mail paraskevi.tavladoraki@uniroma3.it).
†These authors contributed equally to this work.
‡Present address: Department of Biochemical Sciences 'A. Rossi Fanelli', Sapienza University of Rome, Rome, Italy

SUMMARY

Polyamines are involved in several plant physiological processes. In *Arabidopsis thaliana*, five FAD-dependent polyamine oxidases (AtPAO1 to AtPAO5) contribute to polyamine homeostasis. AtPAO5 catalyzes the back-conversion of thermospermine (T-Spm) to spermidine and plays a role in plant development, xylem differentiation, and abiotic stress tolerance. In the present study, to verify whether T-Spm metabolism can be exploited as a new route to improve stress tolerance in crops and to investigate the underlying mechanisms, tomato (*Solanum lycopersicum*) *AtPAO5* homologs were identified (*SlPAO2*, *SlPAO3*, and *SlPAO4*) and CRISPR/Cas9-mediated loss-of-function *slpao3* mutants were obtained. Morphological, molecular, and physiological analyses showed that *slpao3* mutants display increased T-Spm levels and exhibit changes in growth parameters, number and size of xylem elements, and expression levels of auxin- and gibberellin-related genes compared to wild-type plants. The *slpao3* mutants are also characterized by improved tolerance to drought stress, which can be attributed to a diminished xylem hydraulic conductivity that limits water loss, as well as to a reduced vulnerability to embolism. Altogether, this study evidences conservation, though with some significant variations, of the T-Spm-mediated regulatory mechanisms controlling plant growth and differentiation across different plant species and highlights the T-Spm role in improving stress tolerance while not constraining growth.

Keywords: Thermospermine, polyamine oxidase, drought stress tolerance, genome editing for crop improvement, leaf transpiration rate, relative water content, *Solanum lycopersicum*, xylem hydraulic conductivity.

INTRODUCTION

Plants need large amounts of water to live and grow. Vascular plants evolved the xylem for long-distance transport of water and nutrients (Lucas et al., 2013; Sperry, 2003; Venturas et al., 2017). In angiosperms, xylem vessels can be several centimeters long, consisting of coordinated chains of vertically aligned vessel elements that have partially or entirely lost their common end-walls. Xylem vessels are highly interconnected through pits forming a complex network. Pit membranes play a crucial role in

xylem safety, as they can prevent air propagation between conduits, which can disrupt water transport and affect plant growth and survival (Brodersen et al., 2019; Venturas et al., 2017). Water transport through the xylem depends on numerous parameters, such as the anatomical characteristics and spatial distribution of xylem conduits, as well as the number and frequency of network connections. There is a general agreement that wider and longer vessels conduct water more efficiently, but they are also more susceptible to embolism, suggesting a possible trade-off between hydraulic safety and efficiency, although the topic is debated (Brodersen et al., 2019; Lens et al., 2022; Venturas et al., 2017). The understanding of soil-to-leaf water transport can lead to innovative directions to optimize plant water use through breeding programs and biotechnological strategies.

Xylem development is controlled by the integrated action of several endogenous and environmental signals (Aliche et al., 2020; Bollhöner et al., 2012; Jang & Choi, 2018; Milhinhos & Miguel, 2013; Pagliarani et al., 2019; Růžička et al., 2015). Indeed, hormones, small peptides, reactive oxygen species, and Ca^{2+} are essential regulators of this process. Polyamines are also implicated in several processes during xylem differentiation (Fraudentali et al., 2021; Tavladoraki et al., 2016; Tisi et al., 2011; Vera-Sirera et al., 2015). In particular, thermospermine (T-Spm) contributes to the control of xylem differentiation by interfering with auxin and cytokinin signaling pathways (Milhinhos et al., 2020; Milhinhos & Miguel, 2013; Tiburcio et al., 2014; Vera-Sirera et al., 2015). Arabidopsis mutants for *thermospermine synthase* (*ACL5*; Solé-Gil et al., 2019) and *S-adenosyl-methionine decarboxylase 4* genes involved in T-Spm biosynthesis exhibit over-proliferation of xylem vessels and impaired stem elongation and (Cui et al., 2010; Ge et al., 2006; Muñiz et al., 2008), while increased *ACL5* expression levels or exogenous T-Spm suppress xylem differentiation (Baima et al., 2014; Kakehi et al., 2010; Mai et al., 2023; Milhinhos et al., 2013). Furthermore, it has been shown that T-Spm suppresses auxin signaling and auxin-inducible xylem differentiation and that auxin induces *ACL5* expression through a mechanism that maintains T-Spm steady-state levels and finely controls xylem development (Baima et al., 2014; Clay & Nelson, 2005; Milhinhos et al., 2013; Yoshimoto et al., 2012a, 2012b). Genetic studies of suppressor mutants that rescue the dwarf phenotype of *acl5* mutants revealed that a key component of T-Spm function is the basic helix–loop–helix transcription factor SUPPRESSOR OF ACAULIS 51 (SAC51; Imai et al., 2006; Nishii et al., 2023). SAC51 can interact with LONESOME HIGHWAY (LHW), thus inhibiting the formation of heterodimers between LHW and TARGET OF MONOPTEROS 5, which play a central role in xylem formation (Katayama et al., 2015; Vera-Sirera et al., 2015). In particular, T-Spm is believed to activate the translation of *SAC51* mRNA by inhibiting the negative effect of an evolutionarily conserved upstream open reading frame (uORF) of this gene (Cai et al., 2016; Ishitsuka et al., 2019). Mutations of the ribosomal protein genes *RPL10A*, *RACK1A*, and *RPL4A* were also reported to attenuate the inhibitory effect of the *SAC51* uORF in the absence of T-Spm, further supporting T-Spm involvement in ribosomal function (Imai et al., 2008; Kakehi et al., 2015). Recently, it was additionally shown that mutation of a gene encoding a D6-class Jumonji C protein (JMJ22) suppresses the *acl5* phenotype and that JMJ22 stabilizes *SAC51* transcripts through a hitherto unknown mode of action (Matsuo et al., 2022). Furthermore, small nucleolar ribonucleoproteins were suggested to be essential for T-Spm-mediated biological processes (Li et al., 2023).

Numerous reports support the contribution of the different polyamines in plant stress responses through a variety of mechanisms (Montesinos-Pereira et al., 2014; Wang & Liu, 2016; Liu et al., 2015; Pál et al., 2018; Alcázar et al., 2020; Li et al., 2020; Hasan et al., 2021; Upadhyay et al., 2021; Blázquez, 2024). As considered T-Spm, exogenous application induced the expression of pathogenesis-related proteins and improved tolerance to biotic and abiotic stresses (Alcázar et al., 2020; Mo et al., 2015; Sagor et al., 2012; Shinohara et al., 2019). Furthermore, *ACL5* overexpression increased resistance to *Pseudomonas viridiflava* and *Botrytis cinerea*, while on the contrary reduced *ACL5* expression levels increased susceptibility to the fungal pathogen *Verticillium dahliae* and salt stress (Marina et al., 2013; Mo et al., 2015; Shinohara et al., 2019; Zhu et al., 2021). Also, in the non-vascular plant *Marchantia polymorpha*, loss-of-function mutation of *MpACL5* altered responses to heat and salt stress (Furumoto et al., 2024).

Polyamine homeostasis is controlled not only at the level of biosynthesis but also by catabolism, which involves two classes of amine oxidases, the copper amine oxidases and the FAD-dependent polyamine oxidases (PAOs; Tavladoraki et al., 2016; Tiburcio et al., 2014). Plant PAOs display high diversity in substrate specificity, catalytic mechanism, and subcellular localization and belong to three distinct clades (Bordenave et al., 2019; Fincato et al., 2011, 2012; Salvi & Tavladoraki, 2020; Tavladoraki et al., 2016). Clade I includes plant PAOs similar to the intracellular *Arabidopsis thaliana* PAO1 (AtPAO1; Tavladoraki et al., 2006) and the extracellular maize PAO (ZmPAO1; Tavladoraki et al., 1998; Polticelli et al., 2005), together with fungal and algae PAOs. Clade II includes plant PAOs similar to the Arabidopsis polyamine oxidase/dehydrogenase 5 (AtPAO5; Ahou et al., 2014) and animal PAOs (Cervelli et al., 2003; Vujcic et al., 2003). Clade IV includes PAOs similar to the peroxisomal AtPAO2, AtPAO3, and AtPAO4.

AtPAO5 is a cytosolic enzyme catalyzing the back-conversion of spermine (Spm), N^1-acetyl-Spm, and T-Spm to spermidine (Ahou et al., 2014). Furthermore, AtPAO5 is involved in plant development and xylem

differentiation interfering with the cytokinin and auxin signaling pathways by controlling T-Spm levels (Alabdallah et al., 2017; Kaszler et al., 2023). Indeed, loss-of-function *atpao5* mutants and Arabidopsis transgenic plants ectopically expressing *AtPAO5* exhibit differences compared to wild-type plants in T-Spm levels, stem and root elongation, xylem differentiation, and expression levels of auxin- and cytokinin-related genes. In addition, *atpao5* mutants display increased tolerance to drought and salt stress (Sagor et al., 2016; Zarza et al., 2017).

The present study further investigates the contribution of T-Spm metabolism to plant development and drought stress responses. In particular, the aim of this study was to obtain information on the underlying mechanisms and to verify whether strategies based on polyamine metabolism can be designed to transfer stress tolerance traits into crops. To this end, tomato (*Solanum lycopersicum*) CRISPR/Cas9 mutants for one of the three *AtPAO5-like* genes (*SlPAO3*) were analyzed under well-watered and drought stress conditions. The data obtained allow to hypothesize a role for *SlPAO3* in tomato plant growth and xylem differentiation through the control of T-Spm and auxin homeostasis. Furthermore, they evidence the conservation, though with some significant variations, of the T-Spm-mediated regulatory mechanisms across different plant species. The data suggest also that loss-of-function *SlPAO3* mutations affect plant ability to tolerate drought stress via effects on xylem efficiency (through reducing xylem hydraulic conductivity and thus limiting water loss under water-deficit conditions) and safety (by diminishing vulnerability to embolism).

RESULTS

Three AtPAO5 homologs in *S. lycopersicum*

Sequence homology searches identified three *AtPAO5*-like genes in *S. lycopersicum*, named *SlPAO2* (*Solyc05g018880*), *SlPAO3* (*Solyc07g039310*), and *SlPAO4* (*Solyc12g008850.1.1*). The three genes are intron-less, similar to *AtPAO5* and most other plant *AtPAO5-like* genes that belong to the distinct clade II (Salvi & Tavladoraki, 2020). SlPAO2, SlPAO3, and SlPAO4 share a high overall amino-acid sequence identity with AtPAO5 and with each other (Figure 1a). Furthermore, amino acid sequence alignments revealed that SlPAO4 differs from AtPAO5, SlPAO2, and SlPAO3 in the presence of an additional domain of about 150–160 amino acids (Figure 1a). SlPAO4 homologs were identified in several plants (e.g., *Solanum tuberosum*) but not all (e.g., *Nicotiana tabacum*), of the Solanaceae family, the length of the extra domain being variable (Figure S1). Notably, MEME and associated MAST analysis (Bailey et al., 2015; https://meme-suite.org/) identified the presence of multiple tandem repeats (TRs) of a highly conserved motif of 17 amino acids in the extra domain of SlPAO4 homologs (Figure 1b,c; Figure S1), these TRs being distinct from the common TRs known to occur in plant proteins (Kamel et al., 2021; Sharma & Pandey, 2016). The identification of SlPAO4 homologs only in a subgroup of Solanaceae suggests the recent evolution of this type of PAO.

SlPAO2, SlPAO3, and *SlPAO4* expression pattern

It was previously shown that *AtPAO5* expression levels are higher in roots than in leaves and stems (Alabdallah et al., 2017). Similarly, in the present study, quantitative real-time RT-PCR (RT-qPCR) analysis showed higher *SlPAO2*, *SlPAO3*, and *SlPAO4* expression levels in roots than in shoots (Figure 2). Moreover, it showed that T-Spm treatment upregulates *SlPAO4* in shoots and roots (Figure 2). Conversely, *SlPAO2* and *SlPAO3* are not significantly regulated by T-Spm, *SlPAO3* being only slightly downregulated in shoots (Figure 2). On the other hand, *SlPAO2* and *SlPAO3*, but not *SlPAO4*, are downregulated by drought stress (Figure 2). The gene expression data, together with the amino acid sequence analysis, suggest functional similarities among the three genes (mainly between *SlPAO2* and *SlPAO3*), but also functional divergence (mainly of *SlPAO4* from *SlPAO2* and *SlPAO3*).

Generation of CRISPR/Cas9-mediated *slpao3* mutant lines

To study the contribution of T-Spm metabolism to tomato developmental and defense processes, *SlPAO3* was chosen as a representative member of the putative T-Spm specific *SlPAO2-SlPAO4* gene family. To obtain *slpao3* mutants through CRISPR/Cas9 technology, two *SlPAO3*-specific *gRNAs* (*gRNA1* and *gRNA2*; Figure S2) were designed and assembled into a construct adopting a polycistronic *tRNA-gRNA* (*PTG*) strategy (Figure S2b; Xie et al., 2015). Several tomato plants mutated in *SlPAO3* target 2, but not in target 1, were recovered (Table S1), and two lines (-*slpao3-a* and *slpao3-b*) were selected for further studies.

The *slpao3-a* line brings a mutated *SlPAO3* gene with a homozygous in-frame deletion of 24 nucleotides resulting in a deletion of eight amino acids (amino acids 426 to 433; Figure S2d), which is expected to result in a non-functional enzyme, as evidenced by the structural models of the wild-type protein and the SlPAO3-a mutant obtained using trRosettaX (Figure S3). In detail, the overall fold of these models is essentially identical and well superimposable to that of the hSMOX crystal structure (PDB code 7OXL; Diaz et al., 2022) taken as a reference (Figure S3). Furthermore, the 426–433 segment, deleted in the SlPAO3-a mutant, is located at the level of a surface loop and thus could appear not detrimental to the overall fold of the protein. However, a detailed comparative analysis of the structural models revealed that this loop is an essential part of the FAD binding domain (Figure S4, top panels). In particular, the 426–433 segment acts as a plug of the cavity hosting the FAD cofactor, with residues Leu432,

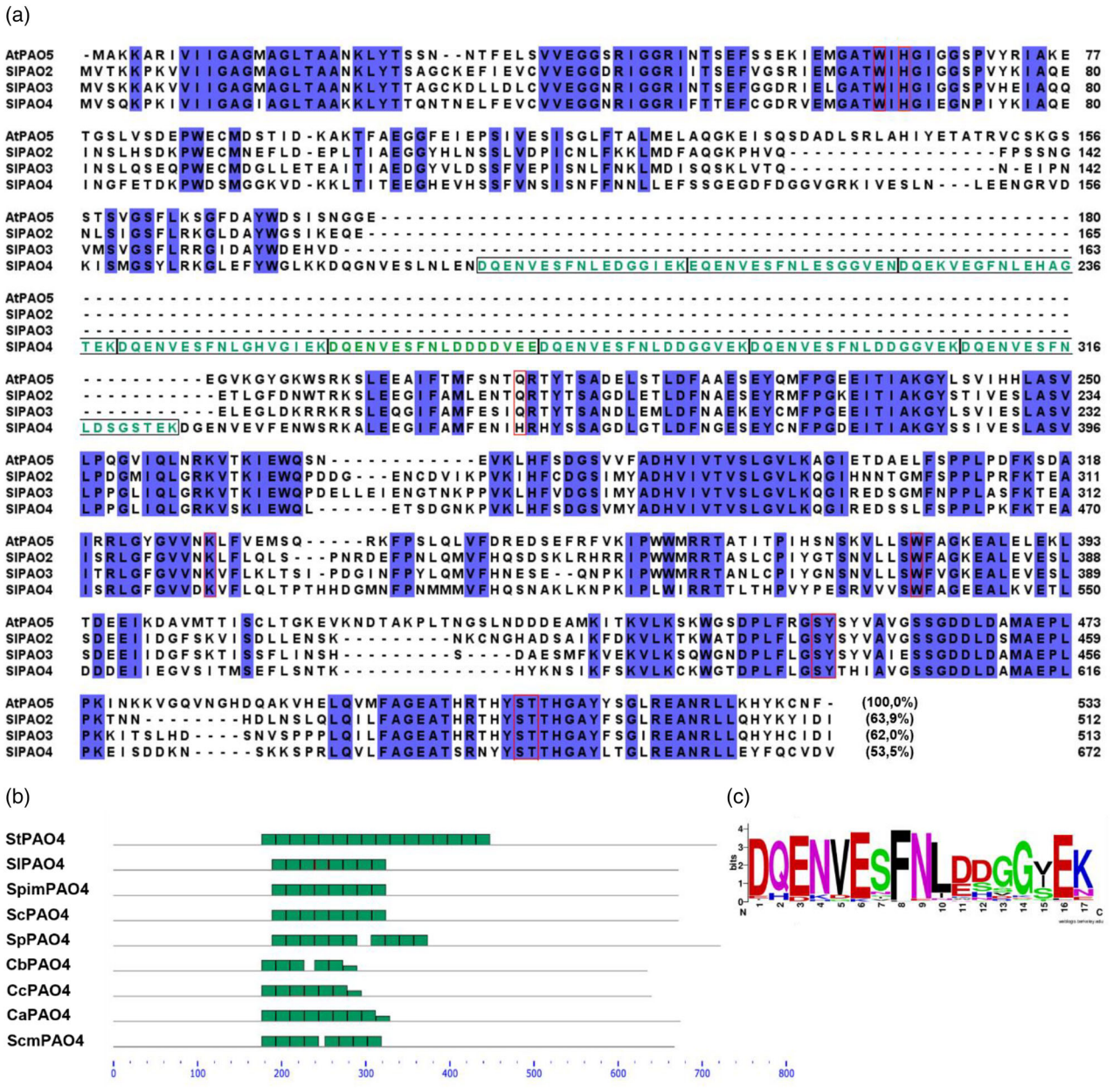

Figure 1. Amino acid sequence analysis of AtPAO5 homologs in Solanaceae species.
(a) Sequence alignment of SlPAO2, SlPAO3, SlPAO4, and AtPAO5. Sequence alignment was performed with CLUSTALW2. The numbering of amino acid residues is shown on the right. Residues of the catalytic site (Ahou et al., 2014; Polticelli et al., 2005) are marked with red boxes. The repeated motif (17 amino acids long) in SlPAO4 is marked with black boxes, and the residues are shown in green color. The numbers in parentheses indicate the percentage of amino-acid sequence identity of SlPAO2, SlPAO3, and SlPAO4 to AtPAO5.
(b) Identification of a conserved and repeated motif in SlPAO4 homologs. The block diagram (green boxes) shows the best non-overlapping tiling of motif identified in the nine SlPAO4 homologs by MEME and associated MAST analysis (https://meme-suite.org/). The height of the block indicates the match significance, with taller blocks being more significant than shorter ones.
(c) Logo of the conserved motif. The overall height of the stack indicates the sequence conservation at that position, while the height of symbols within the stack indicates the relative frequency of each amino acid at that position. Sc, *Solanum chilense*; Scm, *Solanum commersonii*; Sl, *Solanum lycopersicum*; Sp, *Solanum pennellii*; Spim, *Solanum pimpinellifolium*; St, *Solanum tuberosum*; Ca, *Capsicum annuum*; Cb, *Capsicum baccatum*; Cc, *Capsicum chinense*.

Phe433, and Leu434 establishing hydrophobic interactions that appear critical for the stability of the FAD binding domain (Figure S4, bottom panels). Thus, the lack of this loop in the SlPAO3-a mutant likely leads to defective binding of the FAD cofactor and consequently to perturbation of the overall protein structure.

The *slpao3-b* line is characterized by a mutated *SlPAO3* gene with a homozygous out-of-frame deletion of

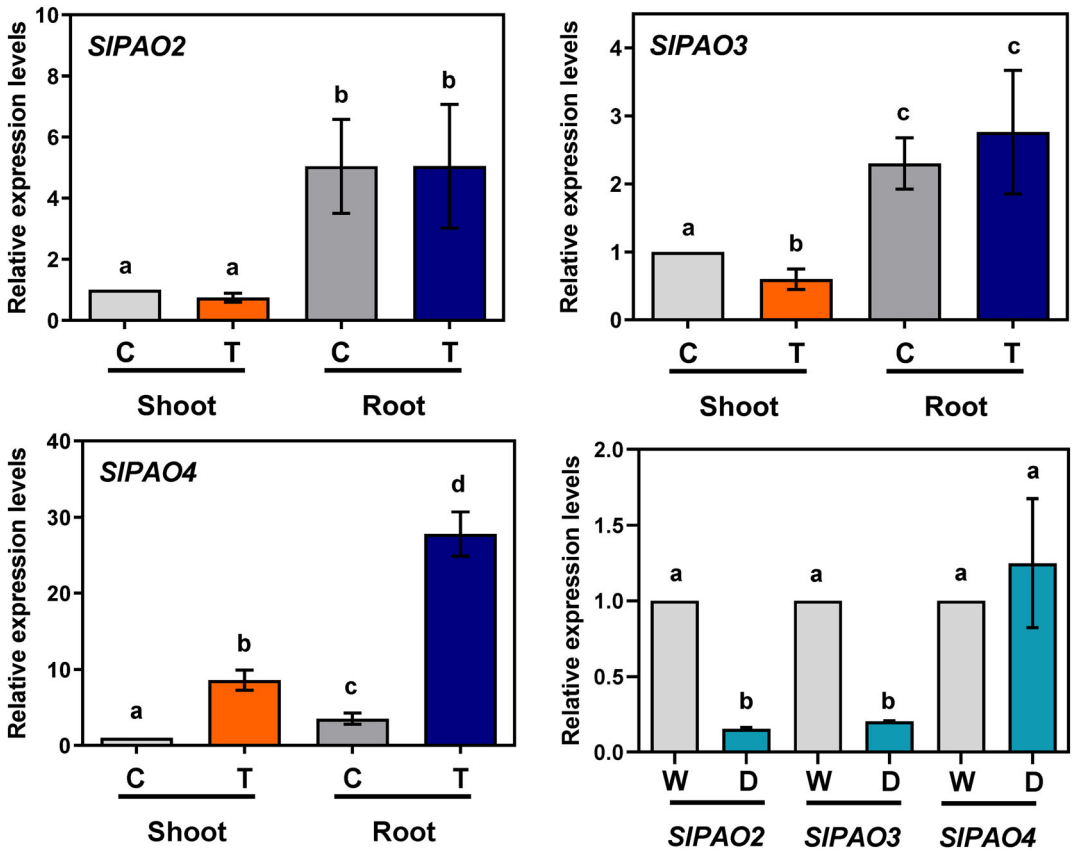

Figure 2. Regulation of *SlPAO2*, *SlPAO3*, and *SlPAO4* gene expression by T-Spm and drought stress.
For analysis of the effect of T-Spm on gene expression, shoots and roots of 7-day-old tomato seedlings were treated (T) or not (C) with 100 μM T-Spm for 24 h and analyzed by RT-qPCR. Values are means of three independent repetitions ± SE. For drought stress, leaves of 4-week-old tomato plants grown in soil under well-watered conditions (W) or following water withholding for 12 days (D). Leaves from three different plants were used for each analysis. A representative experiment out of three independent repetitions is shown. Relative expression levels are presented as fold-changes ($2^{-\Delta\Delta Ct}$) from controls. Different letters above the columns indicate statistically significant differences (one-way ANOVA; $P < 0.05$).

1 nt (at position 1299 of the *SlPAO3* gene), which is also expected to encode a non-functional enzyme, truncated at amino acid position 432 and bearing an extra domain of seven amino acids at the C′ terminus (Figure S2d).

The *slpao3-a* and *slpao3-b* mutants were analyzed for potential off-target mutations. Sequencing analysis of PCR products from six selected potential off-target sites presenting the highest probability score (≥0.1; Table S2) evidenced no mutation or indel in the two mutants as compared to the wild-type plants (Figure S5). These results indicate high *gRNA2* target specificity.

SlPAO3 contributes to T-Spm, auxin, and gibberellin homeostasis in tomato plants

Analysis of polyamine levels in both leaves and stems evidenced that *slpao3-a* and *slpao3-b* mutants have increased T-Spm levels compared to wild-type plants (Figure 3). On the contrary, no statistically significant difference in putrescine (Put), spermidine (Spd), and Spm levels was observed among the different tomato genotypes (Figure S6). These data suggest that *SlPAO3* specifically contributes to T-Spm homeostasis in tomato plants, as *AtPAO5* does in Arabidopsis plants (Alabdallah et al., 2017).

In Arabidopsis and *Populus* plants, it was shown that the *thermospermine synthase* gene (*ACL5*; Knott et al., 2007; Takano et al., 2012) is regulated by T-Spm through a negative feedback loop (Baima et al., 2014; Kakehi et al., 2008, 2010; Milhinhos et al., 2013). A similar regulatory mechanism operates in tomato plants as T-Spm treatment downregulates two *ACL5* homologs (*SlACL5-1* and *SlACL5-2*; Figure 4). On the contrary, a third tomato *ACL5* homolog (*SlACL5-3*) is upregulated by T-Spm (Figure 4), probably for fine regulation of T-Spm levels. Of note, *SlACL5-1*, *SlACL5-2*, and *SlACL5-3* expression levels are higher in roots than in shoots (Figure 4), similar to *SlPAO2*, *SlPAO3*, and *SlPAO4* expression levels (Figure 2).

SlPAO3, contributing to T-Spm homeostasis, participates in the feedback mechanism regulating *SlACL5-1* and *SlACL5-2*. Indeed, RT-qPCR analyses showed that *SlACL5-1* and *SlACL5-2* expression levels are downregulated in the

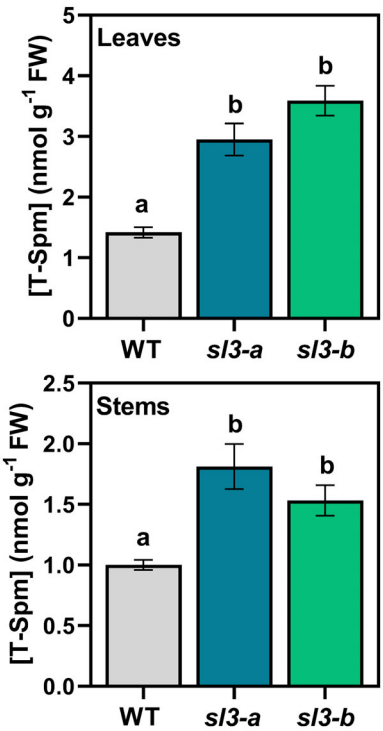

Figure 3. T-Spm levels in *slpao3-a* and *slpao3-b* mutants.
T-Spm levels were determined in leaves and stems of the third internode (from above) of 6-week-old *slpao3-a* (*sl3-a*) and *slpao3-b* (*sl3-b*) mutants, and wild-type (WT) tomato plants. Values are means of three independent repetitions ± SE ($n = 5$). Different letters above the columns indicate statistically significant differences (one-way ANOVA; $P < 0.05$).

slpao3-a and *slpao3-b* mutants in shoots (Figure 5) and roots (Figure S7). On the contrary, no difference in *SlACL5-3* expression levels was observed between *slpao3* mutants and wild-type plants (Figure 5). In addition, no difference was observed between *slpao3* mutants and wild-type plants in *SlPAO2*, *SlPAO3*, and *SlPAO4* expression levels (Figure 5). These data suggest that *SlPAO3* gene disruption does not affect *SlPAO3* transcription and mRNA stability. They also indicate that the increase in T-Spm levels in *slpao3* mutants compared to wild-type plants is not sufficient to upregulate *SlPAO4* and *SlACL5-3* expression, whereas it appears high enough to downregulate *SlACL5-1* and *SlACL5-2*.

RT-qPCR analyses were also performed on the tomato homologs of the Arabidopsis *PIN1* and *PIN6* auxin efflux carrier genes (*SlPIN1* and *SlPIN6*, respectively) that play an important role in auxin homeostasis and distribution (Blilou et al., 2005; Cazzonelli et al., 2013; Sawchuk et al., 2013; Verna et al., 2015) and are regulated by T-Spm (Tong et al., 2014). Data evidenced that *SlPIN1* and *SlPIN6* genes are downregulated by T-Spm (Figure 4) and that they display lower expression levels in *slpao3* mutants than in wild-type plants in both shoots and roots (Figure 5; Figure S7). These data suggest that T-Spm and its metabolism interfere with auxin homeostasis in tomato plants, as in Arabidopsis and *Populus* plants (Clay & Nelson, 2005; Milhinhos et al., 2013; Takano et al., 2012; Tong et al., 2014; Vera-Sirera et al., 2010; Yoshimoto et al., 2012a, 2012b).

The RT-qPCR analyses also showed that T-Spm treatment decreases the expression levels of the gibberellin (GA) biosynthetic gene *SlGA20ox1* and increases those of the GA deactivation gene *SlGA2ox4* (Yamaguchi, 2008; Figure S8), suggesting that T-Spm also interferes with GA homeostasis. This may be due to the effect of T-Spm in auxin homeostasis, the auxin and GA signaling pathways being highly interconnected (Yamaguchi, 2008). However, a direct effect of T-Spm on GA biosynthesis and signal transduction cannot be excluded. Despite the increased T-Spm levels, the *slpao3* mutants present increased *SlGA20ox1* expression levels compared to the wild-type plants (Figure S8), which indicates perturbations in GA homeostasis and probable activation of the feedback homeostatic mechanisms controlling it (Yamaguchi, 2008) in the mutants. On the contrary, no significant difference in *SlGA2ox4* expression levels was observed in the *slpao3* mutants compared to the wild-type plants (Figure S8).

SlPAO3 is involved in the control of plant growth and xylem differentiation

Morphological observations evidenced that the *slpao3-a* and *slpao3-b* mutants have longer stems than the wild-type plants, due to increased internode elongation (Figure 6a,b), which may reflect the observed perturbations in auxin and GA homeostasis. Instead, no difference was observed in the number of internodes and the total leaf area between *slpao3* mutants and wild-type plants (Figure 6c). Transverse sections of stems (Figure 7a,b) and roots (Figure S9) showed that the *slpao3* mutants have a lower number of xylem elements than wild-type plants. In addition, the *slpao3* mutants display thinner cell walls in xylem elements than wild-type plants, as suggested by the differences in the intensity of the cell-wall lignin autofluorescence among the different genotypes (Figure 7a). These differences in xylem differentiation among the different genotypes are probably due to differences in T-Spm levels and consequent alterations in auxin and GA homeostasis. Indeed, T-Spm treatment reduced the number of xylem elements and reverted the observed differences in root xylem differentiation between *slpao3* mutants and wild-type plants (Figure S9a,b). The *slpao3* mutants also display a smaller proportion of large vessels (>1200 μm^2) than wild-type plants (Figure 7c). These data suggest that hydraulic conductivity may be affected in *slpao3* mutants compared to wild-type plants. Indeed, both theoretical calculation and experimental data evidenced lower hydraulic conductivity in *slpao3* mutants than in wild-type plants (Figure 8). These data are consistent with

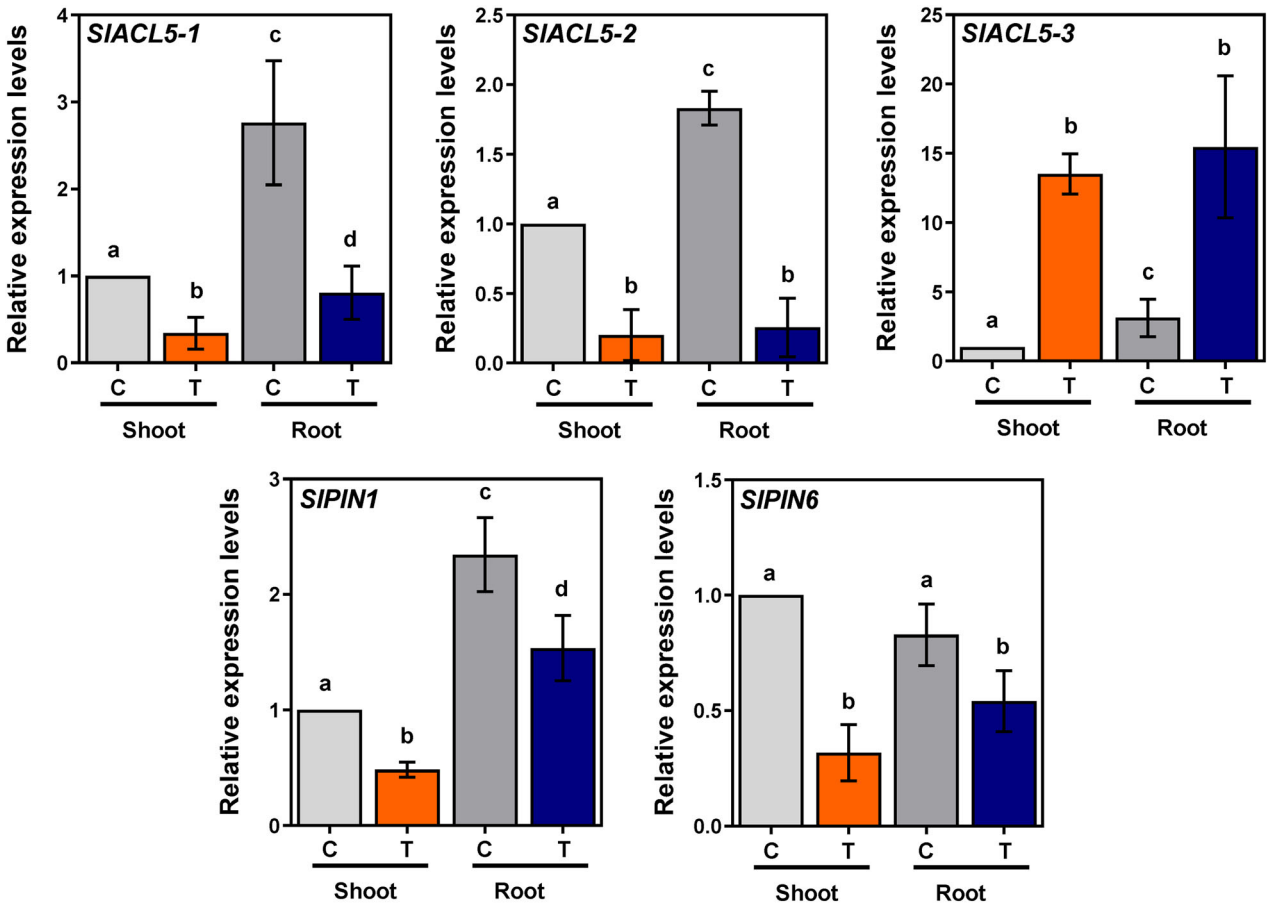

Figure 4. T-Spm mediated regulation of genes involved in T-Spm biosynthesis and auxin transport.
Expression levels were analyzed by RT-qPCR in shoots and roots of 7-day-old tomato seedlings treated (T) or not (C) with 100 μM T-Spm for 24 h. Relative expression levels are presented as fold-changes ($2^{-\Delta\Delta Ct}$) from the shoots of control plants. Values are means of three independent repetitions ± SE. Different letters above the columns indicate statistically significant differences (one-way ANOVA; $P < 0.05$). Similar results were obtained in the leaves of 4-week-old plants.

previous reports correlating perturbations in auxin transport and signaling with changes in xylem differentiation and hydraulic conductivity (Andrade et al., 2022; Fàbregas et al., 2015; Johnson et al., 2018).

The *slpao3* mutant lines exhibit improved tolerance to drought stress

The role of T-Spm metabolism and *SlPAO3* in drought stress responses was investigated by completely interrupting irrigation of *slpao3* mutants and wild-type plants. Of note, drought stress does not affect T-Spm levels, only the amount of Put being increased under these conditions (Figure S10). In this way, the observed differences in T-Spm levels between the wild-type and mutant plants under well-watered conditions are maintained also under drought stress conditions. Plant observation during drought evidenced that wild-type plants present more severe wilting symptoms than *slpao3-a* and *slpao3-b* mutants (Figure 9a; Figure S11). In addition, measurements of relative water content (RWC; Figure 9b) and leaf surface temperature (Figure 9c,d) at various percentages of soil humidity showed that leaf water loss under drought conditions was slower in *slpao3* mutants than in wild-type plants. These data demonstrate that *slpao3* mutants experience less water stress than wild-type plants.

Under well-watered conditions, *slpao3* mutants exhibit lower stomatal conductance (Figure 10a) than wild-type plants, as observed by leaf gas exchange measurements. This trend is inverted under water-limited conditions, with the *slpao3* mutants exhibiting a slower reduction in stomatal conductance with decreasing soil humidity compared to the wild-type plants (Figure 10a). The lower stomatal conductance rate under well-watered conditions and the higher one under drought stress observed in *slpao3* mutants compared to wild-type plants translated into parallel changes in transpiration rates (Figure 10b; Figure S12), as expected due to similar environmental evaporative conditions (temperature and relative humidity) to which plants were exposed during

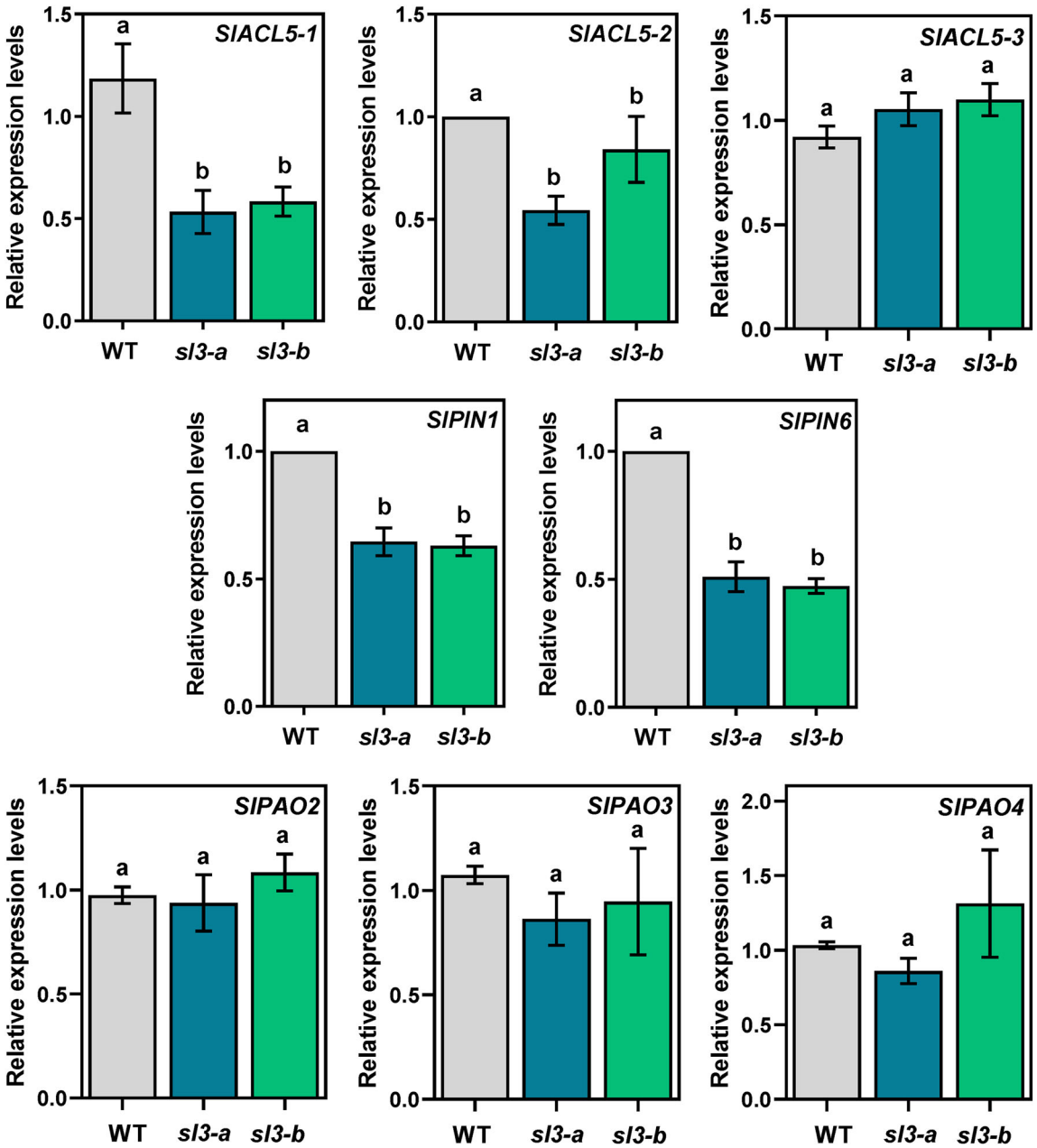

Figure 5. Expression levels of genes involved in T-Spm metabolism and auxin transport in *slpao3* mutants.
Expression levels were analyzed by RT-qPCR in shoots of 9-day-old *slpao3-a* (*sl3-a*), *slpao3-b* (*sl3-b*), and wild-type (WT) tomato genotypes. Relative expression levels are presented as fold-changes ($2^{-\Delta\Delta Ct}$) from WT plants. Values are means of three independent repetitions ± SE. Different letters above the columns indicate statistically significant differences ($P < 0.05$; one-way ANOVA).

experiments. Additionally, *slpao3* mutants maintained higher (i.e., less negative) Ψ_{leaf} values than wild-type plants under water-deficit conditions (Figure 10c). These differences in stomatal conductance, transpiration rate, and water potential between wild-type and mutant plants cannot be attributed to differences in stomatal density or index among genotypes (Figure S13). Furthermore, it was shown that exogenous T-Spm does not affect stomatal conductance (Figure S14). Hence, these data overall suggest that the differences between the wild-type plants and the *slpao3* mutants in stomatal conductance and transpiration rate may be related to hydraulic limitations imposed on stomatal aperture by differences in stem hydraulic conductivity (Figure 8).

To verify whether the *slpao3* mutants display differences from wild-type plants in morpho-anatomical traits

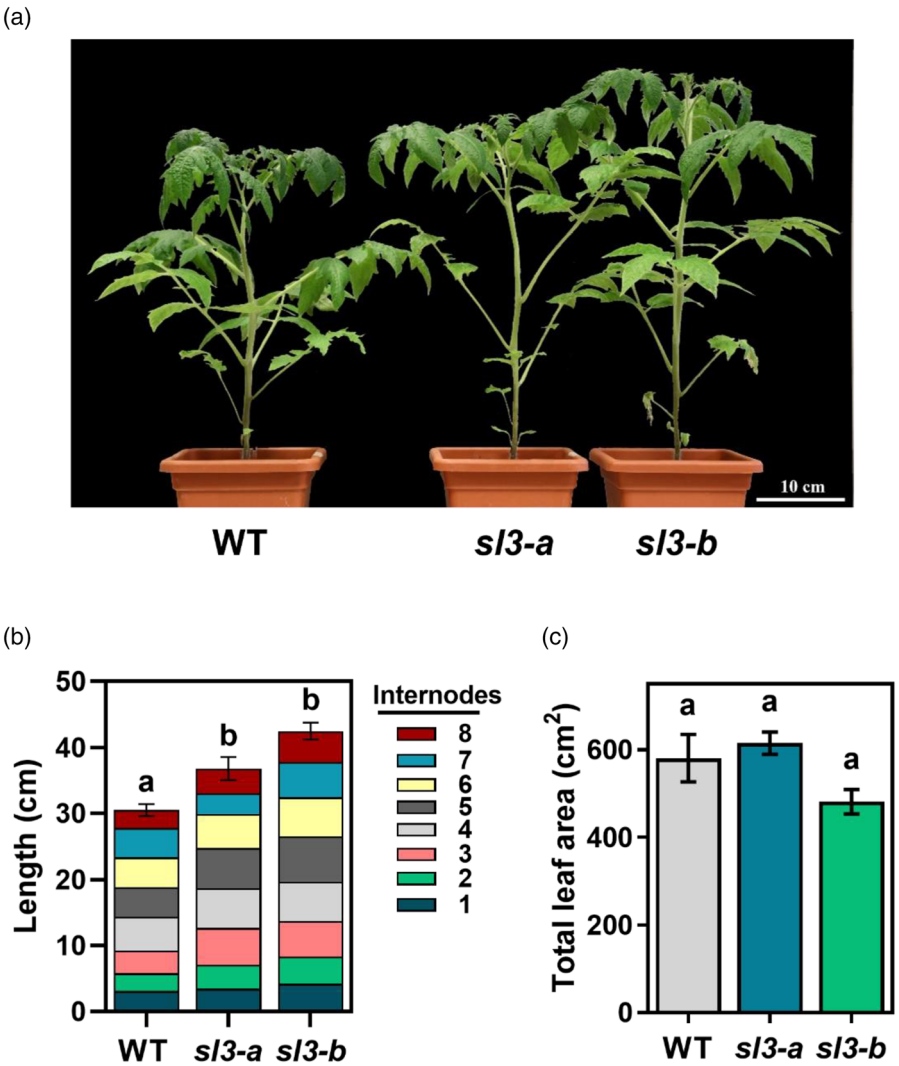

Figure 6. Phenotypical analysis of *slpao3* mutants.
(a) Representative photos of the different tomato genotypes.
(b) Length of the different internodes in the various tomato genotypes. Internode numbering starts from the base of the stem. Bars indicate SEM of the total stem length values.
(c) Total leaf area of the different tomato genotypes. A representative experiment is shown. Different letters above the columns indicate statistically significant differences ($P < 0.05$; one-way ANOVA). WT: wild-type tomato plants; *sl3-a*: *slpao3-a* mutant; *sl3-b*: *slpao3-b* mutant.

that can contribute to the reduced water-loss rate under drought stress conditions, leaf dry matter content (LDMC) and root surface area were determined. These analyses showed no significant difference between *slpao3* mutants and wild-type plants (Figure S13). The leaf osmotic potential at full turgor (π_0) was also measured and the leaf water potential at turgor loss point (Ψ_{tlp}) was calculated (Figure S13), as these physiological traits are strongly linked to drought tolerance (Bartlett et al., 2012; Petruzzellis et al., 2019). These analyses evidenced no statistically significant difference between *slpao3* mutants and wild-type plants and suggested that the increased tolerance to water deficit of *slpao3* mutants does not involve mechanisms related to osmotic adjustments. This conclusion is further supported by data from analysis of the levels of the osmoprotectant proline (Alvarez et al., 2022), which is known to accumulate in response to water or salt stress and is also accepted as a marker of the level of stress perceived by the plants (Le et al., 2022; Pagliarani et al., 2019; Verslues & Sharma, 2010). This analysis revealed that the increase of proline levels during water-deficit progression was lower in *slpao3* mutants than in wild-type plants (Figure 10d). These data further support the notion that *slpao3* mutants undergo less stress than wild-type plants while confirming that *slpao3* stress tolerance is likely not correlated to osmoregulation.

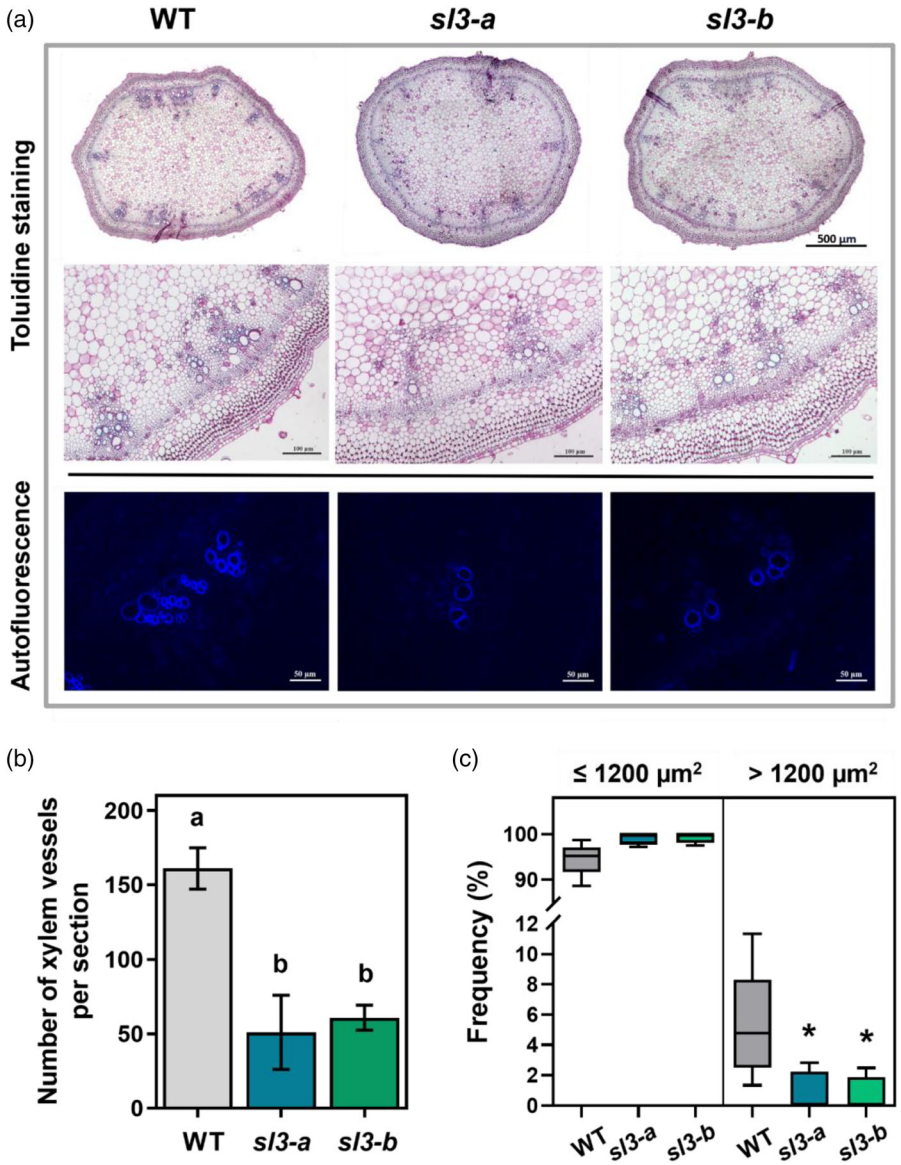

Figure 7. Morphological characteristics of *slpao3* mutants.
(a) Histological analysis of stem transverse sections (at the second internode from the apex) of 6-week-old *slpao3* mutants. Samples were examined under bright-field illumination (toluidine blue staining) and UV light (autofluorescence of cell-wall phenolics). All images were obtained under the same conditions.
(b) Number of xylem elements in stem transverse sections of *slpao3* mutants. Different letters above the columns denote statistically significant differences ($P < 0.05$; one-way ANOVA).
(c) Frequency distribution of cross-sectional area of the xylem elements in the stems of the different tomato genotypes. The xylem elements of the first internode from above were divided into two classes according to their cross-sectional area ($\leq 1200\ \mu m^2$, $>1200\ \mu m^2$) and the percentage of xylem elements in each class (frequency) was calculated. Over 25 bundles from minimum of five different plants of each genotype were analyzed. Asterisks indicate statistically significant differences from the wild-type plants ($P < 0.05$; one-way ANOVA and Student's *t*-test). WT: wild-type tomato plants; *sl3-a*: *slpao3-a* mutants; *sl3-b*: *slpao3-b* mutants.

Drought stress can induce xylem embolism, which disrupts the root-to-leaf water supply. Measurements of the percentage loss of hydraulic conductivity (PLC) evidenced that *slpao3* mutants are significantly less vulnerable to xylem embolism than wild-type plants, at least under moderate stress conditions (Figure 11), thus confirming a higher degree of drought tolerance.

DISCUSSION

Drought stress affects plant growth and survival, reducing crop yield. Plants cope with drought using different strategies, which can be divided into three main classes: (i) drought escape through anticipation of transition from the vegetative to the reproductive stage; (ii) dehydration

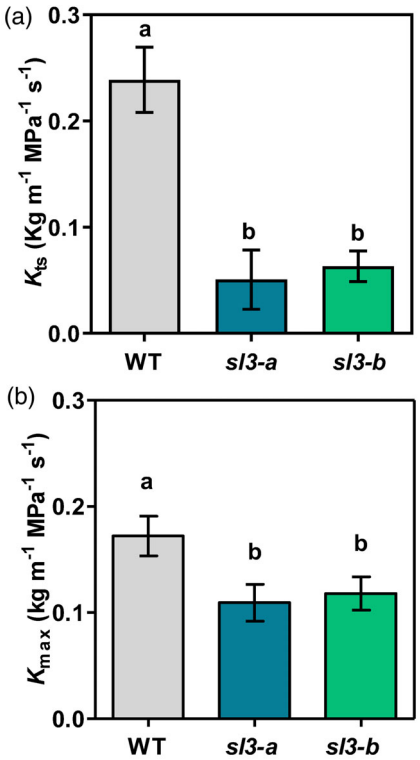

Figure 8. Xylem hydraulic conductivity in *slpao3* mutants.
(a) Theoretical specific hydraulic conductivity (K_{ts}) of the xylem vessels. To calculate K_{ts}, theoretical hydraulic conductivity (K_t) obtained from a modified Hagen–Poiseuille equation (Tyree & Ewers, 1991) was normalized to the area of the stem cross section ($n \geq 5$ per genotype).
(b) Actual hydraulic conductivity (K_{max}) of the xylem vessels under well-watered conditions. Different letters above the columns indicate statistically significant differences ($P < 0.05$; Student's *t*-test; $n \geq 5$ per genotype). WT: wild-type tomato plants; *sl3-a*: *slpao3-a* mutants; *sl3-b*: *slpao3-b* mutants.

tolerance through metabolic adjustments; and (iii) dehydration avoidance through maintenance of a relatively high water content even under low soil water availability by reducing transpiration, limiting shoot growth, and/or increasing root elongation (Blum & Tuberosa, 2018; Kooyers, 2015; Martignago et al., 2020).

Here, the contribution of SlPAO3 and T-Spm to plant responses to drought was investigated. Data show that loss-of-function mutations of *SlPAO3* result in improved drought tolerance. Indeed, *slpao3* mutants showed less severe wilting symptoms, higher water content, and less negative Ψ_{leaf} values than wild-type plants under water shortage (Figure 9; Figure 10; Figure S11). Furthermore, *slpao3* mutants displayed a slower drought-induced reduction in stomatal conductance and transpiration rate, together with a slower drought-induced increase in leaf temperature and proline levels than wild-type plants (Figure 9; Figure 10; Figure S12), suggesting that these mutants undergo less stress than wild-type plants. The drought tolerance of *slpao3* mutants, which is likely correlated with the drought-induced downregulation of *SlPAO3* (Figure 2), maybe a consequence of the reduced xylem hydraulic conductivity (Figure 8) that limits stomatal conductance and transpiration rate (Figure 10; Figure S12). In turn, the lower xylem hydraulic conductivity can be attributed to the reduced number of xylem elements (Figure 7; Figure S9) and the smaller proportion of large vessels in *slpao3* mutants (Figure 7c) compared to wild-type plants. Instead, the increased drought tolerance of *slpao3* mutants likely does not involve mechanisms related to the regulation of stomatal movement by T-Spm, which was ineffective in promoting stomatal closure (Figure S14) and cannot be explained by differences in stomatal density or index, the two parameters being identical in the different genotypes (Figure S13). As a result of this hydraulic limitation effect, the lower transpiration rate of *slpao3* mutants apparently limits excessive water loss under drought conditions, delaying stress symptoms as compared to wild-type plants (Figure 12). Thus, *SlPAO3* mutation mediates increased tolerance to water shortage by favoring a dehydration avoidance strategy (Fang & Xiong, 2015; Kooyers, 2015; Martignago et al., 2020). Notably, drought tolerance mechanisms related to xylem differentiation and water transport efficiency were also observed in previous studies (Illouz-Eliaz et al., 2020; Zhang et al., 2018), in agreement with the central role of xylem in plant growth and survival. Here, it is further shown that *slpao3* mutants present reduced vulnerability to xylem embolism compared to wild-type plants (Figure 11), which may also contribute to the improved drought tolerance (Figure 12). The reduced vulnerability to xylem embolism of *slpao3* mutants is likely associated with the narrower xylem conduits, without excluding the involvement of other structural and/or metabolic alterations.

Plants function under resource limitations and biophysical constraints imposed by external and/or internal molecular and biochemical networks. These constraints lead to trade-offs whereby one trait depends on and is constrained by others (Karasov et al., 2017; Laitinen and Nikoloski, 2022). For example, growth-defense trade-offs associated with defense mechanisms against pathogens and abiotic stresses often occur at the expense of growth and yield. Interestingly, drought tolerance mediated by *SlPAO3* mutation is not associated with growth penalties, at least under growth chamber conditions. Indeed, the *slpao3* mutants exhibit only a mild long stem phenotype (probably due to the diminished xylem differentiation and/or the altered auxin and GA homeostasis) while maintaining an unaltered leaf and root area (Figure 6; Figure S13). Thus, the reduction of the hydraulic conductivity in the *slpao3* mutants that likely contributes to the mechanism determining the improved stress tolerance is sufficient to limit excessive water loss under drought stress conditions but not to impair growth and/or to induce a wilty phenotype under

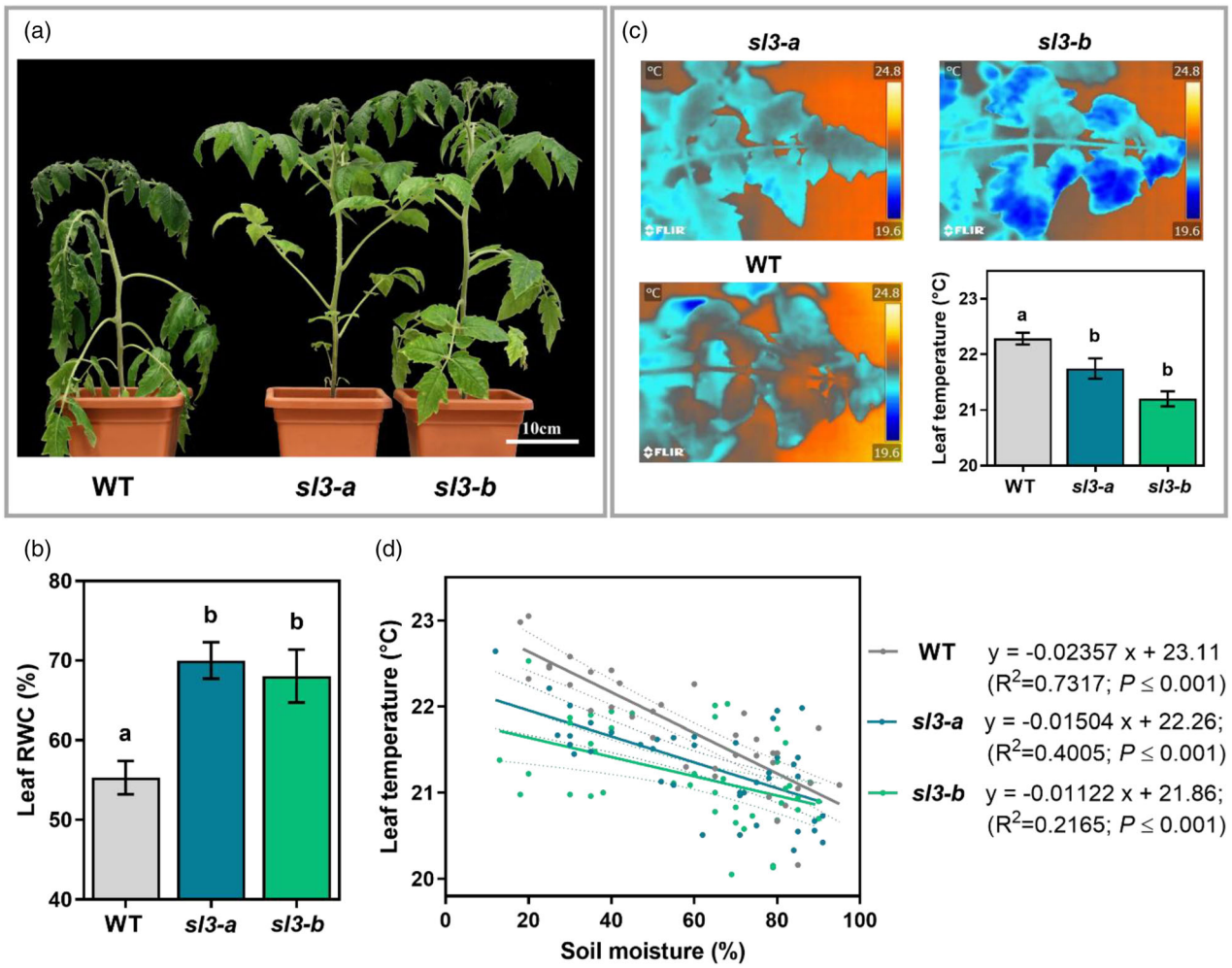

Figure 9. Phenotypic analysis of *slpao3* mutants under drought stress conditions.
(a) Photos of representative 6-week-old plants taken 10 days after the onset of drought stress by completely interrupting irrigation.
(b) Leaf relative water content (RWC) was determined 10 days after the onset of drought stress.
(c) Thermographic pictures of leaves obtained by a thermal camera (FLIR E75) 10 days after the onset of drought stress and respective mean temperatures.
(d) Kinetics of leaf temperature increase with decreasing soil humidity as determined through thermographic pictures. Thermal images were acquired on the third leaf of each plant, before the onset of water stress and then every 2 days, until the end of the experiment. The slope of the correlation curve of the WT plants is statistically different from those of *slpao3-a* and *slpao3-b* mutants, as evidenced by ANCOVA analysis. Different letters above the columns denote statistically significant differences ($P < 0.05$; one-way ANOVA). WT: wild-type tomato plants; *sl3-a*: *slpao3-a* mutants; *sl3-b*: *slpao3-b* mutants.

well-watered conditions, as observed in some *wilty* mutants (Dodd et al., 2008; Koizumi et al., 2007).

The results presented in this study show that *slpao3* mutants display increased T-Spm levels compared to wild-type plants in both leaves and stems (Figure 3), suggesting that SlPAO3 is involved in T-Spm catabolism, similar to its Arabidopsis homolog AtPAO5. The increased T-Spm levels in *slpao3* mutants are probably responsible for the differences from wild-type plants in xylem differentiation observed throughout the entire plant. Indeed, treatment of *slpao3* mutants and wild-type plants with exogenous T-Spm reverted these differences. The effect of T-Spm on xylem differentiation can be attributed to the effect of T-Spm on auxin distribution and GA homeostasis, as indicated by the altered expression levels of *SlPIN1* and *SlPIN6*, as well as of *SlGA20ox1* and *SlGA2ox4*, in *slpao3* mutants and tomato wild-type plants treated with T-Spm compared to control plants (Figure 4; Figure 5; Figure S7; Figure S8). The effect of T-Spm on auxin transport and xylem differentiation of tomato plants is similar to that observed in Arabidopsis and *Populus* (Alabdallah et al., 2017; Milhinhos et al., 2013). Furthermore, similar to Arabidopsis, tomato displays a feedback mechanism regulating T-Spm homeostasis and *SlACL5* expression levels, in which *SlPAO3* participates. Indeed, *slpao3* mutants and T-Spm-treated wild-type tomato plants present a reduction in *SlACL5-1* and *SlACL5-2* expression levels compared to the controls (Figure 4; Figure 5) which, however, is not

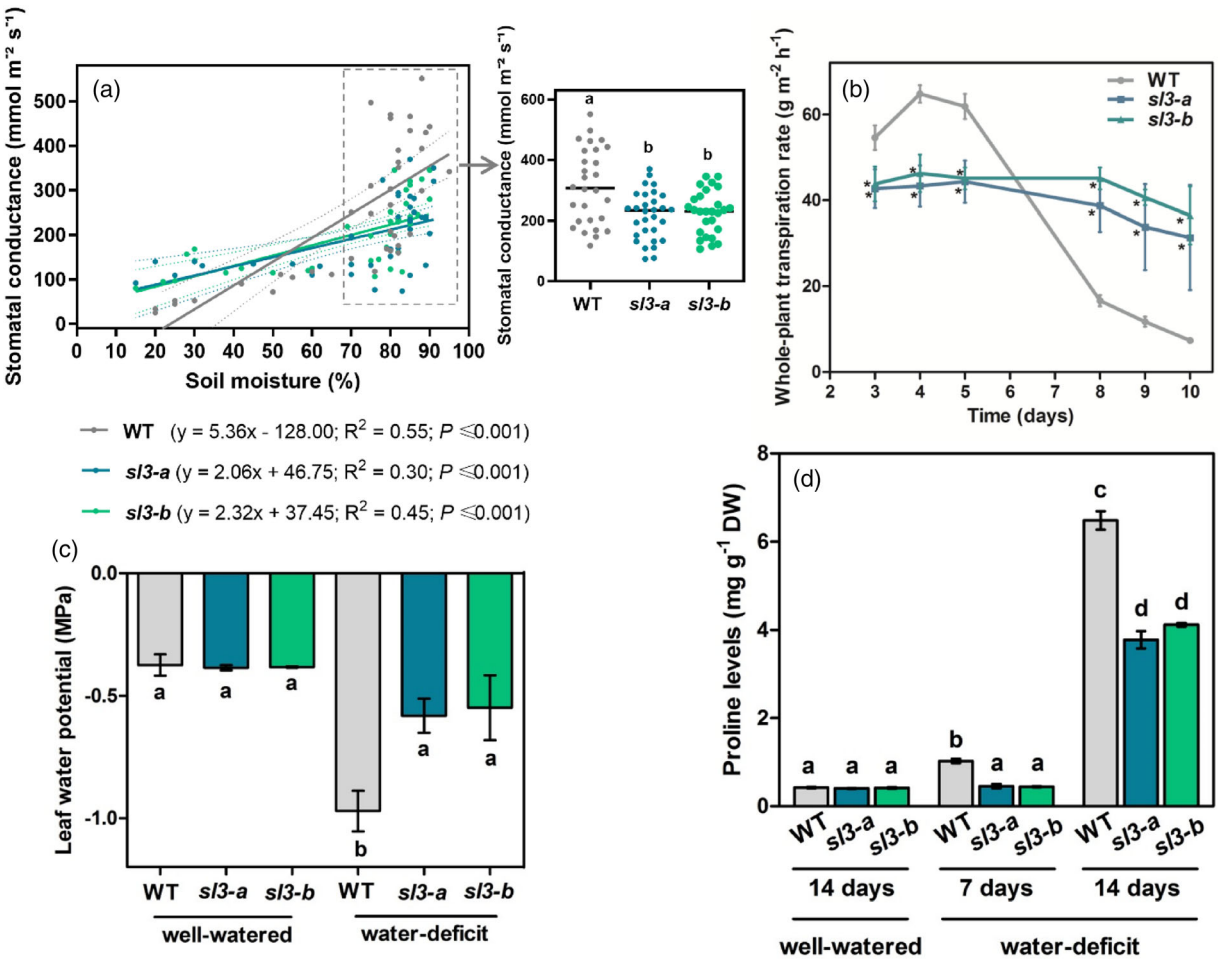

Figure 10. Hydraulic parameters and proline content in *slpao3* mutants under well-watered and drought stress conditions.
(a) Stomatal conductance of the different tomato genotypes at various soil humidity conditions. Stomatal conductance was determined through measurement of CO_2/H_2O gas exchange in leaves of the different tomato genotypes. The slope of the correlation curve of WT plants is statistically different from those of *slpao3-a* and *slpao3-b* mutants, as evidenced by ANCOVA analysis. The insert shows stomatal conductance under conditions of high soil humidity (≥70%).
(b) Whole-plant transpiration rates through gravimetric determination of water-loss kinetics. Asterisks indicate statistically significant differences from the wild-type plants at the corresponding time point ($P < 0.05$; one-way ANOVA).
(c) Leaf water potential of the different tomato genotypes under well-watered and water-stress conditions (10 days after onset of water-withholding).
(d) Proline content in the different tomato genotypes under well-watered and water-stress conditions. Different letters above or below the columns and the scatter dot blots denote statistically significant differences ($P < 0.05$; one-way ANOVA). Representative experiments out of at least three repetitions are shown. WT: wild-type tomato plants; *sl3-a*: *slpao3-a* mutants; *sl3-b*: *slpao3-b* mutants.

sufficient to restore T-Spm levels in the *slpao3* mutants. These observations suggest conservation of the regulatory mechanisms controlling T-Spm homeostasis, auxin transport, and xylem differentiation across different plant species. Nevertheless, unlike Arabidopsis which has a single *ACL5* gene, tomato has three *SlACL5* genes with high sequence similarity to each other and the Arabidopsis *ACL5* (58% - 72%), the *SlACL5-3* being differently regulated by T-Spm from *SlACL5-1* and *SlACL5-2* (Figure 4). Similarly, while Arabidopsis has a single *AtPAO5* gene, tomato has three *AtPAO5* homologs that display differences among them in the regulation of gene expression. These differences between Arabidopsis and tomato are probably due to recent events of gene duplication and change of function and may suggest different physiological roles for the three *SlACL5* and the three *AtPAO5*-like *SlPAO* genes. They also suggest the need for extremely fine regulation of T-Spm levels in tomato plants, considering the relevant role of this polyamine in xylem differentiation and hormone signaling.

Analysis of polyamine levels in tomato plants under well-watered and drought stress conditions showed that drought stress increases Put levels but does not affect those of Spd, Spm, and T-Spm (Figure S10). These data seem to partially contradict previous data indicating variations of Spm and Spd levels under drought stress

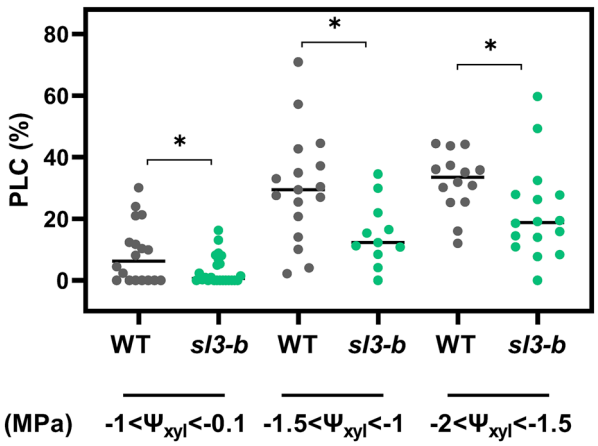

Figure 11. Percentage loss of hydraulic conductivity (PLC) in *slpao3* mutant plants under drought stress conditions.
PLC was determined in stems of 6-week-old *slpao3* mutants (*sl3-b*) and wild-type plants (WT) subjected to drought stress by completely interrupting irrigation. PLC was calculated from hydraulic conductivity measurements at different stem water potential ranges (Ψ_{xyl}, MPa). Asterisks indicate statistically significant differences with respect to the corresponding values of the WT plants (Student's *t*-test, $P < 0.05$).

(Montesinos-Pereira et al., 2014; Upadhyay et al., 2021; Wang et al., 2023). These differences may depend on the plant species and genotype analyzed, as well as on the duration, severity, and mode of drought stress (Montesinos-Pereira et al., 2014; Wang et al., 2023). It was further shown here that T-Spm levels are not affected by drought stress (Figure S10) even though *SlPAO2* and *SlPAO3* genes are downregulated under these conditions (Figure 2) and T-Spm levels were previously shown to be reduced under salt stress conditions (Naka et al., 2010). These data reflect the complex regulatory mechanisms controlling polyamine homeostasis.

All three AtPAO5-like *SlPAO* genes, similar to the three *SlACL5* genes and the *SlPIN1* and *SlPIN6* genes, exhibit higher expression levels in roots than in shoots (Figure 2), suggesting an important role of these genes in root physiology. However, except for differences in xylem differentiation, and despite these differences, no significant change in root growth was observed in *slpao3* mutants compared to wild-type plants. This may be due to gene redundancy and/or the contribution of these genes to different aspects of root physiology.

No information on the tissue-specific expression pattern of *SlPAO3* is available so far. However, the effect of *SlPAO3* gene disruption on xylem differentiation allows hypothesizing expression in xylem cells during vascular differentiation as was previously reported for *AtPAO5* and *ACL5* in Arabidopsis plants (Alabdallah et al., 2017; Clay & Nelson, 2005; Muñiz et al., 2008).

SlPAO2, SlPAO3, and SlPAO4 share high overall amino-acid sequence identity. Despite this, SlPAO4 displays an additional domain characterized by the presence of TRs. The function of these TRs has yet to be discovered, but they may have a regulatory role (Kajava, 2012; Sharma & Pandey, 2016). Biochemical studies on the catalytic

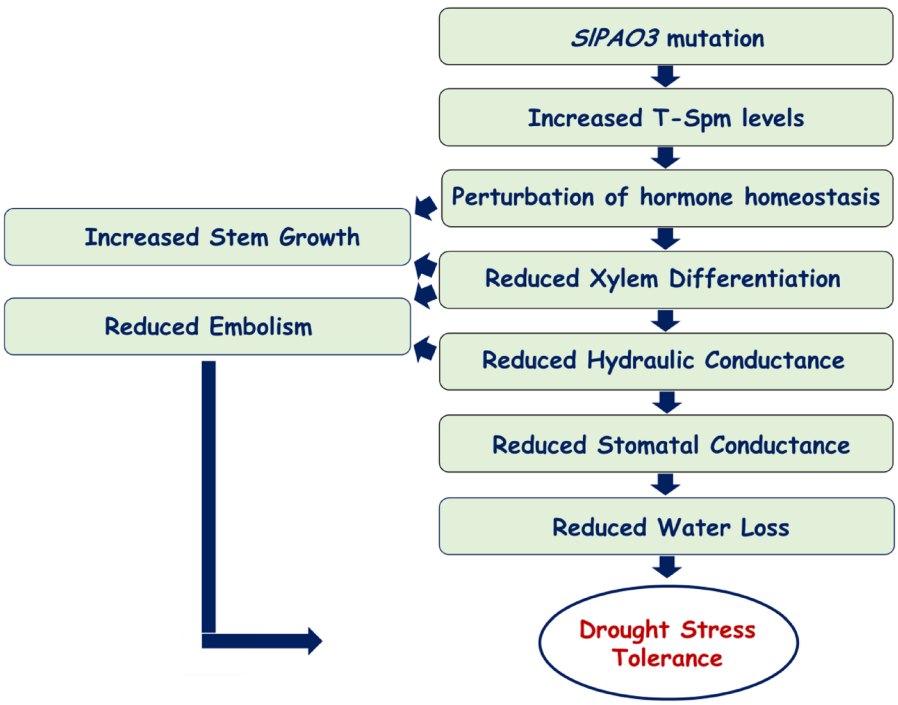

Figure 12. Model of the underlying mechanisms in the SlPAO3-mediated improved tolerance to drought stress.

properties of the three tomato AtPAO5 homologs are necessary to determine substrate specificity and catalytic mechanism, as well as to verify the TR effect on the catalytic reaction.

SlPAO2, *SlPAO3*, and *SlPAO4* present similarities to each other in the regulation of gene expression, but also important differences. In particular, in agreement with previous reports (Hao et al., 2018), both *SlPAO2* and *SlPAO3* genes were shown here to be downregulated by drought stress and not significantly controlled by T-Spm, *SlPAO3* being only slightly downregulated by T-Spm in shoots (Figure 2). *SlPAO2* and *SlPAO3* are also similarly regulated by various stimuli (e.g., various abiotic stresses, polyamine, and hormones), except by cold treatment under which only *SlPAO3* is upregulated (Hao et al., 2018). Unlike *SlPAO2* and *SlPAO3*, *SlPAO4* expression is not affected by drought stress while being upregulated by T-Spm (Figure 2). These data suggest that *SlPAO2* and *SlPAO3* may have similar, though likely not identical, physiological roles, but different from those of *SlPAO4*. This needs to be addressed by characterization of *slpao2* and *slpao4* mutants to determine the specific contribution of each of the three genes in the control of polyamine levels, xylem differentiation, and different developmental and defense processes. Characterization of *slpao2slpao3* and *slpao3slpao4* double mutants is also necessary to analyze gene redundancy effects and verify whether it is possible to further increase T-Spm levels in tomato plants, despite the homeostatic mechanisms, and further improve plant ability to tolerate drought stress.

In conclusion, the present study suggests that genetic manipulation of polyamine metabolism may provide crops with improved tolerance to drought stress without growth penalties. Further studies are in progress to better understand the underlying mechanisms, analyze gene redundancy effects, and unravel the contribution of T-Spm metabolism to different developmental and stress response processes.

EXPERIMENTAL PROCEDURES

Plant material and growth conditions

Tomato (*Solanum lycopersicum*) plants cv Money Maker were used throughout this study. Plants were grown in a controlled growth chamber at 23°C under a 16-h/8-h light/dark photoperiod with a photosynthetic photon flux density (PPFD) of 100–150 μmol m^{-2} sec^{-1}. Seeds were first sterilized and stratified for 4 days at 4°C and then placed on agar plates (0.8% w/v) containing Murashige and Skoog basal medium with Gamborg's vitamins and 3% (w/v) sucrose (MS). For RT-qPCR analysis following T-Spm treatment, 5-day-old seedlings grown on MS agar plates were transferred to MS liquid medium for 24 h. After the addition of fresh medium, seedlings were treated with 100 μM T-Spm. For drought stress, plants were grown in pots of 400 ml or 2.5 L until they produced two (*c.* 4-week-old plants; RT-qPCR analysis) to five (*c.* 6-week-old plants; phenotypical analyses) expanded leaves. Drought stress was imposed by withholding irrigation. Progression of drought stress was monitored on the basis of severity of wilting symptoms. Wilting was scored for 15–30 days after onset of drought on a scale from 10 to 100: 10–20%, very mild wilting in basal leaves; 20–40%, mild wilting in basal internodes; 40–60%, moderate turgor loss in lower internodes; 60–80%, high turgor loss in upper and lower internodes; 80–100%, very high to complete turgor loss of all leaves.

Generation of CRISPR/Cas9-mediated mutagenesis constructs, tomato plant transformation, and mutant selection

Two single-guide RNAs (*gRNA1* and *gRNA2*) targeting the *SlPAO3* gene were designed using the ChopChop CRISPR web tool (https://chopchop.cbu.uib.no/). The two *gRNAs* were assembled in one construct applying a *PTG* strategy (Xie et al., 2015) and the Golden Gate cloning system (Engler et al., 2008; Weber et al., 2011) and using the *pGTR* plasmid (Xie et al., 2015; Table S3). The assembled *SlPAO3-PTG* cassette was put under the promoter of Arabidopsis *U6 snRNA* gene (*AtU6p*; *AtU6p::PTG* construct) obtained from the *pICSL01009::AtU6p* vector (Nekrasov et al., 2013) and introduced inside the *pICH47751* vector (Weber et al., 2011; Table S3). The *AtU6p::PTG* construct was assembled with *2x35S-5′UTR::hCas9::NOST* and *NOSp::NPTII* constructs within the *pAGM4723* binary vector using the *pICH47742::2x35S-5′UTR-hCas9*(*STOP*)*-NOST* (Belhaj et al., 2013) and *pICSL11024* (*pICH47732::NOSp-NPTII-OCST*) plasmids, respectively, as well as the *pICH50892* plasmid (Weber et al., 2011) to provide a linker sequence (Table S3). The final binary vector was introduced into *Agrobacterium tumefaciens* strain *C58C1* (*pCH32*) (Hellens et al., 2000; Wroblewski et al., 2005) by electroporation. This strain was used to transform tomato plants (Van Eck et al., 2019; van Roekel et al., 1993) and several independent kanamycin-resistant T0 transgenic lines were selected. Transgenic lines were analyzed by PCR for the presence of *Cas9* and/or *neomycin phosphotransferase* (*NPTII*) genes. *Cas9*-positive lines were further genotyped by *SlPAO3* sequencing. Several homozygous *slpao3* mutant lines were identified in T1 and T2 generations (Table S1), and two independent mutant lines (*slpao3-a* and *slpao3-b*) were selected for further analyses. In the case of the *slpao3-b* line, the *Cas9* construct was segregated out in the T2 generation. All oligonucleotides used for construct preparation and molecular characterization of the transgenic plants are listed in Table S4.

Extraction of genomic DNA from plant tissue

Genomic DNA was extracted from young leaves following homogenization with 200 μl of extraction buffer (2% SDS, 250 mM NaCl, 25 mM EDTA, 200 mM Tris pH 7.5). The homogenate was heated for 10 min at 60°C and centrifuged at 13 000 ***g*** to remove debris. Then, an equal volume of isopropanol was added to the supernatant and, after 5 min of incubation, the mix was centrifuged for 15 min at 13 000 ***g***. The resulting pellet was washed with cold 70% ethanol, dried, and resuspended in water.

Identification of the repeated motifs in SlPAO4 homologs

Xstream (https://amnewmanlab.stanford.edu/xstream/) analysis was initially conducted on each of the nine SlPAO4 homologs of Solanaceae found by BLASTp (https://blast.ncbi.nlm.nih.gov/Blast.cgi?PAGE=Proteins) and related repeated motifs of 17 amino acids were identified. MEME analysis (https://meme-suite.

org/meme/tools/meme) was then conducted to evaluate the presence of a common repeated motif among the nine SlPAO4 homologs. MEME was run with the option anr, which assumes that each sequence may contain any number of non-overlapping occurrences of each motif. MEME identified two closely related repeated motifs of 17 amino acids that MAST (https://meme-suite.org/meme/tools/mast) analysis merged into one.

RT-qPCR analyses

Total RNA was extracted using the Trizol reagent (Qiagen S.r.l., Milan, Italy) according to the manufacturer's protocol. Genomic DNA was degraded using the RNase-Free DNase Set (Qiagen). For RT-qPCR, cDNA synthesis and PCR amplification were carried out using the GoTaq 2-Step RT-qPCR System (Promega Corporation, Madison, WI, USA). The PCR reactions were run in a Corbett RG6000 (Corbett Life Science, Qiagen) as follows: at 95°C for 2 min, followed by 40 cycles of 95°C for 3 sec and 60°C for 30 s. At least three independent biological replicates were performed for each experiment, to obtain mean values of relative expression levels from the different biological replicates. Relative expression levels were presented as fold-changes ($2^{-\Delta\Delta Ct}$) from the controls. The genes for actin (Solyc04g011500.3.1) and SGN-U316474 (*SlSAND*; Expósito-Rodríguez et al., 2008) were used as reference genes. Gene-specific oligonucleotides used are listed in Table S4.

Analysis of potential off-target mutations

Potential off-target loci associated with *gRNA2* were identified using CRISPR-P 2.0 (http://crispr.hzau.edu.cn/CRISPR2/) and CRISPOR (http://crispor.org) website tools and those with a high probability score (≥0.1) were selected for further analyses (Table S2). The genomic regions flanking the selected putative off-target sites (510–590 bp) were PCR amplified using specific primers (Table S4) and the resulting amplicons were subjected to sequencing analysis.

Determination of polyamine levels

Polyamine levels were determined in leaves and stems by gas chromatography–mass spectrometry (Ahou et al., 2014).

Histological analyses

Root and stem segments were embedded in Technovit 7100 resin (Heraeus Kulzer GmbH, Wehrheim, Germany), and transverse sections (10 μm) were made using a Microm HM330 microtome (Bio Optica Milano S.p.A., Milano, Italy). For histochemical localization of lignin, sections were stained in 0.05% (w/v) toluidine blue solution and then observed under a Zeiss Axiophot 2 microscope equipped with a Leica DFC450C digital camera. Sections were also examined under UV light to observe the autofluorescence of cell-wall phenolics. Images were used to quantify the number and cross-sectional area of the xylem elements.

Measurement of leaf and root surface area

Total leaf and root surface area was calculated by photographing the whole foliage and root apparatus (in the latter case after thorough washing) of 6-week-old tomato plants and analyzing the images by ImageJ (http://rsb.info.nih.gov/ij/).

Thermal image acquisition and processing

Thermal images were acquired using a thermal camera (FLIR E75 series; FLIR Systems, Inc.) with a reading accuracy of ±2%, reading temperature from −20 to +650°C, image resolution of 320 × 240 pixels, and thermal sensitivity <0.03°C. Images were acquired by photographing the third composite leaf (starting from the apex) every 2 days, before and after the onset of drought until the end of the experiment. The false-color images indirectly show the leaf water status (Costa et al., 2013). Images were analyzed using proprietary software (FLIR Thermal Studio Suite). Each composite leaf was subdivided into smaller areas, using dedicated software options, and the temperature of each area was measured. The temperature of the surface of each leaf was calculated as the average of all areas.

Determination of stomatal conductance and transpiration rate

Leaf stomatal conductance and transpiration rate were recorded by CI-340 Handheld Photosynthesis System (CID Bio-Science, Washington, DC, USA). All measurements were done 8–10 h after the beginning of the light cycle under a PPFD of 120 μmol m^{-2} sec^{-1}.

Whole-plant transpiration measurements

Whole-plant transpiration rates were determined using 4-week-old potted plants. Pots were sealed to prevent evaporation from the surface of the growth medium and their weight was monitored using a balance every 1 h (during the light period) for a period of 10 days after the onset of drought. The daily plant transpiration rate (weight loss in 1 h) was calculated from the difference in whole-plant weight between two time points (8–10 h after the beginning of the light cycle) normalized to total leaf area.

Determination of leaf relative water content

Leaf relative water content (RWC) was measured on the third leaf (from the apex) of each plant under well-watered and drought conditions as previously described (Sade et al., 2009). Immediately after leaf detachment, fresh weight (FW) was measured. Leaves were rehydrated by immersion of petioles in water for 18 h at room temperature under low light conditions, and turgid weight (TW) was recorded. Dry weight (DW) was measured after drying the leaves at 90°C for 3 days. RWC was calculated as:

$$RWC = \frac{(FW - DW)}{(TW - DW)} \times 100$$

Calculation of theoretical specific hydraulic conductivity

The theoretical hydraulic conductivity (K_t; mmol m MPa^{-1} sec^{-1}) was calculated based on the modified Hagen–Poiseuille equation (Tyree & Ewers, 1991):

$$K_t = \left(\frac{\pi\rho}{128\mu}\right)\sum_{i=1}^{n}\left(d_i^4\right)$$

where d_i is the diameter (m) of the ith xylem vessel, ρ is the water density in kg m^{-3} (998,2 kg m^{-3} at 20°C), μ is the water viscosity in MPa sec (1.002 10^{-9} MPa sec) and n is the number of xylem vessels in the stem section. K_t was normalized by the area of the cross sections obtained between nodes 5 and 6 (from the apex) to obtain theoretical specific hydraulic conductivity (K_{ts}; mmol m^{-1} MPa^{-1} sec^{-1}).

Estimation of leaf and xylem water potential

Leaf water potential measurements were performed using a pressure chamber (mod. 600 D, PMS Instrument Company, Albany, OR, USA) (Scholander et al., 1965). To estimate xylem water potential (Ψ_{xyl}), leaves from the third or fourth internode (from above) were covered with plastic film and silver foil under dark.

Leaves were then detached from the plant by cutting the petiole with a sharp blade and the water potential was measured.

Estimation of maximum vessel length and mean vessel length

To avoid artifacts due to spurious air entering xylem conduits during sample preparation for hydraulic measurements, maximum vessel length was estimated. This was done by the "air-injection method" as previously described (Wang et al., 2014). In detail, stems of 6-week-old plants were cut at the basal end with a sharp razor blade and connected to a Tygon tubing system. Following re-cutting of the stems at the apical end, air delivered from a pressure chamber instrument (mod. 600 D, PMS Instrument Company) was perfused from the basal end of the stem segments to the apical cut sections while immersed in water at an air pressure of 200 kPa. The stem was progressively shortened by 1 cm cuts at the apical end until the first bubbles emerged from the cut sections, indicating that at least one vessel was cut open at both ends. The length of the remaining stem was recorded as the maximum length of the vessels. The stem was then cut systematically and the air flow rate, which is proportional to the number of vessels extending from one cut end to the apical end of the plant, was measured at different stem lengths. To this end, bubbles flowing out during a time interval were collected in a volumetric cylinder by the water displacement method, and the air volume was measured gravimetrically. Flow rate data were used to calculate mean vessel length (Pan et al., 2015; Figure S15).

Measurement of stem hydraulic conductivity and xylem embolism

Stem hydraulic conductivity was measured in 6-week-old plants either well-watered or dehydrated at different xylem water potentials, as described by Tomasella et al. (2019). Briefly, the main stem was cut at the basal end (1 cm above the soil) and immediately immersed in clean tap water. Following a second short cut made under water next to the previous one, a third cut was made at a distance 1.5-fold longer than the mean vessel length (i.e., 15 cm; Figure S15) to minimize any possible cutting artifact (Torres-Ruiz et al., 2015). After several consecutive cuts made under water at both ends, a 70-mm-long stem segment between nodes 5 and 6 (from above) was obtained and connected to a custom-made hydraulic apparatus. The sample was perfused with a reference 10 mM KCl solution (Nardini et al., 2007) previously degassed and filtered at 0.2 μm. Native stem specific hydraulic conductivity (K_i) was measured gravimetrically under low water pressure conditions (5 kPa, generated by a water head) by collecting the solution at the extremity of the stem segment for 30- to 60-sec intervals in 1.5-ml Eppendorf tubes filled with a piece of sponge. K_i was calculated as:

$$K_i = \frac{M \times L}{A \times t \times P}$$

where M is the mass of the collected perfusion solution (kg), L is the stem segment length (m), A is the area of stem cross section (m^2), t is the duration of solution collection (s), and P is water pressure applied at the sample (MPa).

The stem segment was then flushed for 5 min at high pressure (0.15 MPa) generated in a captive air water tank connected to the apparatus. The duration of the flush was previously checked to be sufficient to remove embolism and to reach the maximum stem hydraulic conductivity (K_{max}), measured as for K_i. Xylem embolism was quantified as percentage loss of hydraulic conductivity (PLC):

$$PLC = 100\left[1-\left(\frac{K_i}{K_{max}}\right)\right]$$

Water potential at turgor loss point

Water potential at the turgor loss point (Ψ_{tlp}) was estimated in leaves of 6-week-old, well-watered, plants as described by Petruzzellis et al. (2019). Two leaves were detached from each plant, one to determine the leaf dry matter content (LDMC; mg g^{-1}) and the other to measure the osmotic potential. LDMC was determined by measuring leaf fresh weight after complete hydration (i.e., turgid weight, TW), through petiole immersion in water for 18 h, and then dry weight (DW) after oven-drying for 24 h at 70°C. LDMC was calculated as:

$$LDMC = \frac{DW}{TW}$$

For osmotic potential measurement, the second leaf was immersed for 2 min in liquid nitrogen while bagged in cling film and then ground into fine pieces. The water potential of the ground leaf material that corresponds to its incorrect osmotic potential at full turgor ($\pi_{0,incorr}$) was measured with a dewpoint hygrometer (Model WP4, Decagon Devices Inc., Pullman, USA). The corrected osmotic potential at full turgor (π_0) was calculated from $\pi_{0,incorr}$ taking into account LDMC as follows:

$$\pi_0 = (0.506 \times \pi_{0,incorr}) - (0.002 \times LDMC)$$

Ψ_{tlp} was finally calculated as:

$$\Psi_{tlp} = 1.312 \times \pi_0 - 0.032$$

Determination of proline levels

Proline content was measured as previously described (Bates et al., 1973) and using L-proline as the standard. Samples from first and second leaves (from the apex) of control and stressed plants were collected and dried at 90°C for 3 days to eliminate water and inactivate enzymes. Then, samples were homogenized in 3% (w/v) 5-sulfosalicylic acid and the absorbance was read at 520 nm. The proline content was expressed as mg/g of DW.

Measurements of stomatal index and density

Stomatal index (stomata number/total number of epidermal cells) and stomatal density were determined by the imprinting technique (Nir et al., 2017). Dental resin (eliteHD+; Zhermack Clinical) was attached to the leaf abaxial side and then removed after drying. The resin epidermal imprints were covered with transparent nail polish, which served as a mirror image of the resin imprint. The nail polish imprints were photographed under a Zeiss Axiolab 5 microscope equipped with a Zeiss Axiocam 208 digital camera.

Measurement of stomatal response to T-Spm treatment

To investigate possible direct effects of T-Spm on stomatal aperture, stomatal conductance was measured as described above following T-Spm treatment. For the treatment, all leaves of 4-week-old plants were sprayed with 1 mM T-Spm and stomatal conductance was registered at various time intervals.

Molecular modeling

The structural models of SlPAO3 wild-type protein and SlPAO3-a mutant were obtained using trRosettaX, an algorithm for protein structure prediction based on a supervised transformer

protein language model used to predict inter-residue two-dimensional geometry. This, in turn, was used to reconstruct the three-dimensional structure of the protein of interest via energy minimization (Wang et al., 2022). The crystal structure of human spermine oxidase (hSMOX; PDB code 7OXL; Diaz et al., 2022) was used as a reference.

Statistical analyses

Statistical analysis was performed by the Microsoft Excel software together with Real Statistics Resource Pack Add-in (https://real-statistics.com/free-download/real-statistics-resource-pack/), and the GraphPad Prism software (version 6.01). Experiments were repeated at least three times and results are expressed as the mean value ± standard error of the mean (SEM). Statistical comparison between groups was performed by unpaired Student's *t*-test, and/or analysis of variance (one-way ANOVA). Statistical analysis of slopes of correlation curves was performed by ANCOVA. *P* values ≤0.05 were regarded as significant.

ACCESSION NUMBERS

The Accession number of genes analyzed in the present study are as follows: AT5g13700 (*AtPAO5*; *Arabidopsis thaliana*), Solyc05g018880 (*SlPAO2*; *S. lycopersicum*), Solyc 07g039310 (*SlPAO3*; *S. lycopersicum*), Solyc12g008850.1.1 (*SlPAO4*; *S. lycopersicum*), Solyc08g061970 (*SlACL5-1*; *S. lycopersicum*), Solyc09g075900 (*SlACL5-2*; *S. lycopersicum*), Solyc07g041300 (*SlACL5-3*; *S. lycopersicum*), Solyc 03g118740 (*SlPIN1*; *S. lycopersicum*), Solyc06g059730 (*SlPIN6*; *S. lycopersicum*), Solyc04g011500.3.1 (*SlACTIN*; *S. lycopersicum*), Solyc03g115810.2.1 (SGN-U316474; *SlSAND*; *S. lycopersicum*), Solyc03g006880.2.1 (*SlGA20ox1*; *S. lycopersicum*), Solyc07g061720.2.1 (*SlGA2ox4*; *S. lycopersicum*), Sopen12g003780 (*SpPAO4*; *Solanum pennellii*), SOLCI007272600_T001 (*ScPAO4*; *Solanum chilense*), Sopim12g008850 (*SpimPAO4*; *Solanum pimpinellifolium*), PGSC0003DMP400000657 (*StPAO4*; *Solanum tuberosum*), KAG5569611.1 (*ScmPAO4*; *Solanum commersonii*), PHT73535.1 (*CaPAO4*; *Capsicum annuum*), PHT52116.1 (*CbPAO4*; *Capsicum baccatum*), PHU08139.1 (*CcPAO4*; *Capsicum chinense*).

ACKNOWLEDGEMENTS

We wish to thank Dr. Luca Nardi (ENEA, Casaccia, Rome, Italy) for providing the thermal camera (FLIR E75) and useful information. We also thank Dr Valerio Foschi for his technical support. The authors acknowledge the financial support of University Roma Tre and the Italian Ministero dell'Università e della Ricerca (MUR): grants to RA (PRIN 2017, CUP F84I19000730005), to PT (PRIN2022, CUP F53D23003950006), and to the Department of Science of University Roma Tre ("Dipartimenti di Eccellenza" 2023-2027). The authors also acknowledge the support of National Biodiversity Future Centre (NBFC) to University Roma Tre, funded by MUR, PNRR, Missione 4 Componente 2, 'Dalla ricerca all'impresa', Investimento 1.4, Project CN00000033. RD is funded by an NBFC research fellowship. RM, DM, and IF benefit from funding FSE REACT-EU, within the program PON "Research and Innovation" 2014-2020 (PON R&I), Action IV.6 "Contratti di ricerca su tematiche Green." This work was also partly supported by the Rome Technopole PNRR, grant M4-C2-Inv. 1.5 CUP F83B22000040006 to RA. In particular, the preparation of the constructs for CRISPR/Cas9-mediated *SlPAO3* mutagenesis was funded by Rome Technopole.

AUTHOR CONTRIBUTIONS

PT designed the research plan with input from MT^2 and AN. RD, RM, RT, MT^2, AM, AI, MT^3, and PT performed the experiments. DM made analyses of mutant sequences. FP performed the protein structural analyses. PT, RD, RM, and MT^3 wrote the manuscript. DM, IF, AC, RA, MT^2, and AN critically reviewed the manuscript.

CONFLICT OF INTEREST

The authors declare that they have no conflict of interest.

DATA AVAILABILITY STATEMENT

All data supporting the findings of this study are available within the paper and within its Supporting information published online.

SUPPORTING INFORMATION

Additional Supporting Information may be found in the online version of this article.

Figure S1. Amino acid sequence of plant SlPAO4 homologs. The additional protein domain in SlPAO4 homologs is highlighted in italic and bold characters. Tandem repeats are indicated in red and green colors.

Figure S2. Schematic diagram of *SlPAO3* gene, vector construction, and CRISPR/Cas9-mediated mutagenesis. (a) Schematic diagram of *SlPAO3* gene and position of target sites 1 and 2. (b) Scheme of the binary vector constructed for CRISPR/Cas9-mediated *SlPAO3* mutagenesis in which the relative position of the *NOSp::NPTII*, *2x35S::hCas9* and *AtU6p::tRNA-gRNA1-tRNA-gRNA2* cassettes is shown. The design is not in scale. (c) *SlPAO3-a* and *SlPAO3-b* genotypes. Sequence of target site 2 is indicated in blue and protospacer adjacent motif (PAM) in red. Black dashed lines indicate base pair deletions. (d) The SlPAO3-a and SlPAO3-b protein isoforms. The deleted sequence in SlPAO3-a isoform is indicated in green, while the extra amino acids at the C terminus of the SlPAO3-b are shown in red. *AtU6p*: promoter of Arabidopsis *U6 snRNA* gene; *2x35SP*: doubled enhanced *CaMV 35S* promoter; *hCas9*: human codon-optimized *Cas9 nuclease* gene; *NOSp*: promoter of *nopaline synthase* gene; *NPTII*: *neomycin phosphotransferase* II gene.

Figure S3. Structural models of SlPAO3 wild-type protein and SlPAO3-a mutant. Ribbon representation of the crystal structure of human spermine oxidase (hSMOX; PDB code 7OXL; Diaz et al., 2022) and of the structural models of SlPAO3 and SlPAO3-a. Structural models were obtained by trRosettaX using hSMOX as a reference. The FAD cofactor is represented as in "spacefill" and colored in magenta.

Figure S4. Comparison of SlPAO3 and SlPAO3-a structural models showing the changes affecting the FAD cofactor molecular environment. Top panels, ribbon representation; central panels, molecular surface representation; bottom panels, enlarged view showing the hydrophobic plug of the FAD binding pocket, formed by Leu432, Phe433, Leu434 residues, present in SlPAO3 and absent in SlPAO3-a mutant. The green arrows highlight the deleted region.

Figure S5. Sequence analysis of the top six potential genome-wide off-target sites in the *slpao3* mutants. The genomic regions flanking the selected putative off-target sites (OFF-A to OFF-F; Table S2) were amplified from *slpao3-a* and *slpao3-b* mutants, and wild-type plants (WT). Resulting amplicons were sequenced and chromatograms at the putative off-target sites are shown. Mismatch nucleotides with respect to the *SlPAO3 gRNA2* (GGAAACGATCCACTCTTCTTGGG) are marked in red, and PAM sites are shown in blue.

Figure S6. Putrescine, spermidine, and spermine levels in *slpao3-a* and *slpao3-b* mutants. Polyamine levels were determined in leaves and stems of the third internode (from above) of 6-week-old *slpao3-a* (*sl3-a*) and *slpao3-b* (*sl3-b*) mutants, and wild-type (WT) tomato plants. Values are means of three independent repetitions ± SE ($n = 3$). Letters above the columns indicate the statistical analysis (one-way ANOVA; $P < 0.05$). Put: putrescine; Spd: spermidine; Spm: spermine.

Figure S7. Expression levels of genes involved in T-Spm biosynthesis and auxin transport in the roots of *slpao3* mutants. Expression levels were analyzed by RT-qPCR in roots of 9-day-old *slpao3-a* (*sl3-a*), *slpao3-b* (*sl3-b*), and wild-type (WT) tomato genotypes. Relative expression levels are presented as fold-changes ($2^{-\Delta\Delta Ct}$) from the control plants. Values are means of three independent repetitions ± SEM. Different letters above the columns indicate statistically significant differences (one-way ANOVA; $P < 0.05$).

Figure S8. Effect of T-Spm on the expression levels of genes involved in gibberellin biosynthesis (*SlGA20ox1*) and deactivation (*SlGA2ox4*). Expression levels were analyzed by RT-qPCR in shoots of 7-day-old tomato wild-type seedlings treated (T) or not (C) with 100 μM T-Spm for 24 h. Expression levels were also analyzed in leaves of 4-week-old *slpao3-a* (*sl3-a*), *slpao3-b* (*sl3-b*), and wild-type (WT) tomato genotypes. Relative expression levels are presented as fold-changes ($2^{-\Delta\Delta Ct}$) from the control plants. Values are means of three independent repetitions ± SEM. Different letters above the columns indicate statistically significant differences (Student's *t*-test, $P < 0.05$).

Figure S9. Morphological characteristics of roots of *slpao3-b* mutants and effect of T-Spm. (a) Histological analysis of root transverse sections under bright-field illumination (toluidine blue staining) and UV light (autofluorescence of cell-wall phenolics). (b) Number of xylem elements in root transverse sections of *slpao3-b* mutants. Root segments from 1 cm below the root-hypocotyl junction of 10-day-old seedlings were analyzed. Different letters above the columns indicate statistically significant differences (one-way ANOVA; $P < 0.05$). WT: wild-type tomato plants; *sl3-b*: *slpao3-b* mutants.

Figure S10. Polyamine levels in *slpao3* mutants and wild-type plants under drought stress conditions. Polyamine levels were determined in the second and third leaves from the apex of 4-week-old *slpao3-a* (*sl3-a*) and *slpao3-b* (*sl3-b*) mutants, and wild-type (WT) tomato plants. Samples were collected from well-irrigated plants ($-0.3\ \text{MPa} < \Psi_{xyl} < -0.1\ \text{MPa}$) and plants for which irrigation was interrupted for 12 days ($-1.0\ \text{MPa} < \Psi_{xyl} < -0.7\ \text{MPa}$). Values are means of at least three different plants ± SE. Different letters above the columns indicate statistically significant differences (one-way ANOVA; $P < 0.05$). Put: putrescine; Spd: spermidine; Spm: spermine; T-Spm: thermospermine.

Figure S11. Levels of leaf wilting in *slpao3* mutants under drought stress conditions. For drought stress, irrigation of 6-week-old plants was completely interrupted and the severity of wilting symptoms was monitored for 15–30 days after onset of drought. A scale of leaf wilting was arbitrarily set up: 10–20%, very mild wilting in basal leaves; 20–40%, mild wilting in basal internodes; 40–60%, moderate turgor loss in lower internodes; 60–80%, high turgor loss in upper and lower internodes; 80–100%, very high to complete turgor loss of all leaves. A representative experiment is shown. WT: wild-type tomato plants; *sl3-a*: *slpao3-a* mutants; *sl3-b*: *slpao3-b* mutants. The wilting levels of the two *slpao3* mutants were statistically different from those of the wild-type (WT) plants for at least 26 days after the start of water withholding (one-way ANOVA; $P < 0.05$; $n \geq 5$ per genotype).

Figure S12. Transpiration rate of the different tomato genotypes at various soil humidity conditions. Transpiration rate was determined through measurement of CO_2/H_2O gas exchange in leaves of the different tomato genotypes. The slope of the correlation curve of wild-type plants (WT) is statistically different from those of *slpao3-a* (*sl3-a*) and *slpao3-b* (*sl3-b*) mutants, as evidenced by ANCOVA analysis. The insert shows transpiration rate under conditions of high soil humidity (≥70%).

Figure S13. Stomatal index, stomatal density, root surface area, leaf dry matter content (LDMC), and leaf water potential at turgor loss point (Ψ_{tlp}) in leaves of *slpao3* mutants and wild-type (WT) tomato plants. Letters above the box and whiskers plots indicate the statistical analysis (one-way ANOVA; $P < 0.05$).

Figure S14. Measurement of stomatal response to T-Spm treatment. All leaves of 4-week-old tomato plants were sprayed with 1 mM T-Spm and stomatal conductance was measured through measurement of CO_2/H_2O gas exchange. Values obtained after 1 h of treatment are shown. Values are means from three different plants ± SEM.

Figure S15. Estimation of maximum and mean vessel length in the different tomato genotypes. Letters above the scatter dot blots indicate the statistical analysis (one-way ANOVA; $P < 0.05$). WT: wild-type tomato plants; *sl3-a*: *slpao3-a* mutants; *sl3-b*: *slpao3-b* mutants.

Table S1. Mutated sequence in *slpao3* mutants.

Table S2. Putative genome-wide off-target sites.

Table S3. Plasmids used for construct preparation and plant transformation.

Table S4. Sequence of oligonucleotides used in this study.

REFERENCES

Ahou, A., **Martignago, D.**, **Alabdallah, O.**, **Tavazza, R.**, **Stano, P.**, **Macone, A.** ***et al.*** (2014) A plant spermine oxidase/dehydrogenase regulated by the proteasome and polyamines. *Journal of Experimental Botany*, **65**, 1585–1603.

Alabdallah, O., **Ahou, A.**, **Mancuso, N.**, **Pompili, V.**, **Macone, A.**, **Pashkoulov, D.** ***et al.*** (2017) The Arabidopsis polyamine oxidase/dehydrogenase 5 interferes with cytokinin and auxin signaling pathways to control xylem differentiation. *Journal of Experimental Botany*, **68**, 997–1012.

Alcázar, R., **Bueno, M.** & **Tiburcio, A.F.** (2020) Polyamines: small amines with large effects on plant abiotic stress tolerance. *Cells*, **9**, 2373.

Aliche, E.B., **Prusova-Bourke, A.**, **Ruiz-Sanchez, M.**, **Oortwijn, M.**, **Gerkema, E.**, **Van As, H.** ***et al.*** (2020) Morphological and physiological responses of the potato stem transport tissues to dehydration stress. *Planta*, **251**, 45.

Alvarez, M.E., **Savouré, A.** & **Szabados, L.** (2022) Proline metabolism as regulatory hub. *Trends in Plant Science*, **27**, 39–55.

Andrade, M.T., **Oliveira, L.A.**, **Pereira, T.S.**, **Cardoso, A.A.**, **Batista-Silva, W.**, **DaMatta, F.M.** ***et al.*** (2022) Impaired auxin signaling increases vein and stomatal density but reduces hydraulic efficiency and ultimately net photosynthesis. *Journal of Experimental Botany*, **73**, 4147–4156.

Bailey, T.L., **Johnson, J.**, **Grant, C.E.** & **Noble, W.S.** (2015) The MEME suite. *Nucleic Acids Research*, **43**, 39–49.

Baima, S., **Forte, V.**, **Possenti, M.**, **Peñalosa, A.**, **Leoni, G.**, **Salvi, S.** ***et al.*** (2014) Negative feedback regulation of auxin signaling by ATHB8/ACL5-BUD2 transcription module. *Molecular Plant*, **7**, 1006–1025.

Bartlett, M.K., **Scoffoni, C.**, **Ardy, R.**, **Zhang, Y.**, **Sun, S.**, **Cao, K. *et al.*** (2012) Rapid determination of comparative drought tolerance traits: using an osmometer to predict turgor loss point. *Methods in Ecology and Evolution*, **3**, 880–888.

Bates, L.S., **Waldren, R.P.** & **Teare, I.D.** (1973) Rapid determination of free proline for water-stress studies. *Plant and Soil*, **39**, 205–207.

Belhaj, K., **Chaparro-Garcia, A.**, **Kamoun, S.** & **Nekrasov, V.** (2013) Plant genome editing made easy: targeted mutagenesis in model and crop plants using the CRISPR/Cas system. *Plant Methods*, **9**, 39.

Blázquez, M.A. (2024) Polyamines: their role in plant development and stress. *The Annual Review of Plant Biology*, **75**. Available from: https://doi.org/10.1146/annurev-arplant-070623-110056

Blilou, I., **Xu, J.**, **Wildwater, M.**, **Willemsen, V.**, **Paponov, I.**, **Friml, J. *et al.*** (2005) The PIN auxin efflux facilitator network controls growth and patterning in Arabidopsis roots. *Nature*, **433**, 39–44.

Blum, A. & **Tuberosa, R.** (2018) Dehydration survival of crop plants and its measurement. *Journal of Experimental Botany*, **69**, 975–981.

Bollhöner, B., **Prestele, J.** & **Tuominen, H.** (2012) Xylem cell death: emerging understanding of regulation and function. *Journal of Experimental Botany*, **63**, 1081–1094.

Bordenave, C.D., **Granados Mendoza, C.**, **Jiménez Bremont, J.F.**, **Gárriz, A.** & **Rodríguez, A.A.** (2019) Defining novel plant polyamine oxidase subfamilies through molecular modeling and sequence analysis. *BMC Evolutionary Biology*, **19**, 28.

Brodersen, C.R., **Roddy, A.B.**, **Wason, J.W.** & **McElrone, A.J.** (2019) Functional status of xylem through time. *Annual Review of Plant Biology*, **70**, 407–433.

Cai, Q., **Fukushima, H.**, **Yamamoto, M.**, **Ishii, N.**, **Sakamoto, T.**, **Kurata, T. *et al.*** (2016) The SAC51 family plays a central role in thermospermine responses in Arabidopsis. *Plant & Cell Physiology*, **57**, 1583–1592.

Cazzonelli, C.I., **Vanstraelen, M.**, **Simon, S.**, **Yin, K.**, **Carron-Arthur, A.**, **Nisar, N. *et al.*** (2013) Role of the Arabidopsis PIN6 auxin transporter in auxin homeostasis and auxin-mediated development. *PLoS One*, **8**, e70069.

Cervelli, M., **Polticelli, F.**, **Federico, R.** & **Mariottini, P.** (2003) Heterologous expression and characterization of mouse spermine oxidase. *The Journal of Biological Chemistry*, **278**, 5271–5276.

Clay, N.K. & **Nelson, T.** (2005) Arabidopsis thick vein mutation affects vein thickness and organ vascularization, and resides in a provascular cell-specific spermine synthase involved in vein definition and in polar auxin transport. *Plant Physiology*, **138**, 767–777.

Costa, J.M., **Grant, O.M.** & **Chaves, M.M.** (2013) Thermography to explore plant-environment interactions. *Journal of Experimental Botany*, **64**, 3937–3949.

Cui, X., **Ge, C.**, **Wang, R.**, **Wang, H.**, **Chen, W.**, **Fu, Z. *et al.*** (2010) The BUD2 mutation affects plant architecture through altering cytokinin and auxin responses in Arabidopsis. *Cell Research*, **20**, 576–586.

Diaz, E., **Adhikary, S.**, **Tepper, A.W.J.W.**, **Riley, D.**, **Ortiz-Meoz, R.**, **Krosky, D. *et al.*** (2022) Structure of human spermine oxidase in complex with a highly selective allosteric inhibitor. *Communications Biology*, **5**, 787.

Dodd, I.C., **Ferguson, B.J.** & **Beveridge, C.A.** (2008) Apical wilting and petiole xylem vessel diameter of the *rms2* branching mutant of pea are shoot controlled and independent of a long-distance signal regulating branching. *Plant & Cell Physiology*, **49**, 791–800.

Engler, C., **Kandzia, R.** & **Marillonnet, S.** (2008) A one pot, one step, precision cloning method with high throughput capability. *PLoS One*, **3**, e3647.

Expósito-Rodríguez, M., **Borges, A.A.**, **Borges-Pérez, A.** & **Pérez, J.A.** (2008) Selection of internal control genes for quantitative real-time RT-PCR studies during tomato development process. *BMC Plant Biology*, **8**, 131.

Fàbregas, N., **Formosa-Jordan, P.**, **Confraria, A.**, **Siligato, R.**, **Alonso, J.M.**, **Swarup, R. *et al.*** (2015) Auxin influx carriers control vascular patterning and xylem differentiation in *Arabidopsis thaliana*. *PLoS Genetics*, **11**, e1005183.

Fang, Y. & **Xiong, L.** (2015) General mechanisms of drought response and their application in drought resistance improvement in plants. *Cellular and Molecular Life Sciences*, **72**, 673–689.

Fincato, P., **Moschou, P.N.**, **Ahou, A.**, **Angelini, R.**, **Roubelakis-Angelakis, K.A.**, **Federico, R. *et al.*** (2012) The members of *Arabidopsis thaliana* PAO gene family exhibit distinct tissue- and organ-specific expression pattern during seedling growth and flower development. *Amino Acids*, **42**, 831–841.

Fincato, P., **Moschou, P.N.**, **Spedaletti, V.**, **Tavazza, R.**, **Angelini, R.**, **Federico, R. *et al.*** (2011) Functional diversity inside the Arabidopsis polyamine oxidase gene family. *Journal of Experimental Botany*, **62**, 1155–1168.

Fraudentali, I., **Rodrigues-Pousada, R.A.**, **Angelini, R.**, **Ghuge, S.A.** & **Cona, A.** (2021) Plant copper amine oxidases: key players in hormone signaling leading to stress-induced phenotypic plasticity. *International Journal of Molecular Sciences*, **22**, 5136.

Furumoto, T., **Yamaoka, S.**, **Kohchi, T.**, **Motose, H.** & **Takahashi, T.** (2024) Thermospermine is an evolutionarily ancestral phytohormone required for organ development and stress responses in *Marchantia polymorpha*. *Plant and Cell Physiology*, **65**, 460–471. Available from: https://doi.org/10.1093/pcp/pcae002

Ge, C., **Cui, X.**, **Wang, Y.**, **Hu, Y.**, **Fu, Z.**, **Zhang, D. *et al.*** (2006) BUD2, encoding an S-adenosylmethionine decarboxylase, is required for Arabidopsis growth and development. *Cell Research*, **16**, 446–456.

Hao, Y., **Huang, B.**, **Jia, D.**, **Mann, T.**, **Jiang, X.**, **Qiu, Y. *et al.*** (2018) Identification of seven polyamine oxidase genes in tomato (*Solanum lycopersicum* L.) and their expression profiles under physiological and various stress conditions. *Journal of Plant Physiology*, **228**, 1–11.

Hasan, M.M., **Skalicky, M.**, **Jahan, M.S.**, **Hossain, M.N.**, **Anwar, Z.**, **Nie, Z.F. *et al.*** (2021) Spermine: its emerging role in regulating drought stress responses in plants. *Cells*, **10**, 261.

Hellens, R., **Mullineaux, P.** & **Klee, H.** (2000) Technical focus: a guide to agrobacterium binary Ti vectors. *Trends in Plant Science*, **5**, 446–451.

Illouz-Eliaz, N., **Nissan, I.**, **Nir, I.**, **Ramon, U.**, **Shohat, H.** & **Weiss, D.** (2020) Mutations in the tomato gibberellin receptors suppress xylem proliferation and reduce water loss under water-deficit conditions. *Journal of Experimental Botany*, **71**, 3603–3612.

Imai, A., **Hanzawa, Y.**, **Komura, M.**, **Yamamoto, K.T.**, **Komeda, Y.** & **Takahashi, T.** (2006) The dwarf phenotype of the Arabidopsis *acl5* mutant is suppressed by a mutation in an upstream ORF of a bHLH gene. *Development*, **133**, 3575–3585.

Imai, A., **Komura, M.**, **Kawano, E.**, **Kuwashiro, Y.** & **Takahashi, T.** (2008) A semi-dominant mutation in the ribosomal protein L10 gene suppresses the dwarf phenotype of the acl5 mutant in *Arabidopsis thaliana*. *The Plant Journal*, **56**, 881–890.

Ishitsuka, S., **Yamamoto, M.**, **Miyamoto, M.**, **Kuwashiro, Y.**, **Imai, A.**, **Motose, H. *et al.*** (2019) Complexity and conservation of thermospermine-responsive uORFs of *SAC51* family genes in angiosperms. *Frontiers in Plant Science*, **10**, 564.

Jang, G. & **Choi, Y.D.** (2018) Drought stress promotes xylem differentiation by modulating the interaction between cytokinin and jasmonic acid. *Plant Signaling & Behavior*, **13**, e1451707.

Johnson, D., **Eckart, P.**, **Alsamadisi, N.**, **Noble, H.**, **Martin, C.** & **Spicer, R.** (2018) Polar auxin transport is implicated in vessel differentiation and spatial patterning during secondary growth in Populus. *American Journal of Botany*, **105**, 186–196.

Kajava, A.V. (2012) Tandem repeats in proteins: from sequence to structure. *Journal of Structural Biology*, **179**, 279–288.

Kakehi, J., **Kawano, E.**, **Yoshimoto, K.**, **Cai, Q.**, **Imai, A.** & **Takahashi, T.** (2015) Mutations in ribosomal proteins, RPL4 and RACK1, suppress the phenotype of a thermospermine-deficient mutant of *Arabidopsis thaliana*. *PLoS One*, **10**, 0117309.

Kakehi, J., **Kuwashiro, Y.**, **Motose, H.**, **Igarashi, K.** & **Takahashi, T.** (2010) Norspermine substitutes for thermospermine in the control of stem elongation in *Arabidopsis thaliana*. *FEBS Letters*, **584**, 3042–3046.

Kakehi, J., **Kuwashiro, Y.**, **Niitsu, M.** & **Takahashi, T.** (2008) Thermospermine is required for stem elongation in *Arabidopsis thaliana*. *Plant & Cell Physiology*, **49**, 1342–1349.

Kamel, M., **Kastano, K.**, **Mier, P.** & **Andrade-Navarro, M.A.** (2021) REP2: a web server to detect common tandem repeats in protein sequences. *Journal of Molecular Biology*, **433**, 166895.

Karasov, T.L., **Chae, E.**, **Herman, J.J.** & **Bergelson, J.** (2017) Mechanisms to mitigate the trade-off between growth and defense. *Plant Cell*, **29**, 666–680.

Kaszler, N., **Benkő, P.**, **Molnár, Á.**, **Zámbori, A.**, **Fehér, A.** & **Gémes, K.** (2023) Absence of Arabidopsis polyamine oxidase 5 influences the cytokinin-induced shoot meristem formation from lateral root primordia. *Plants*, **12**, 454.

Katayama, H., **Iwamoto, K.**, **Kariya, Y.**, **Asakawa, T.**, **Kan, T.**, **Fukuda, H. *et al.*** (2015) A negative feedback loop controlling bHLH complexes is

involved in vascular cell division and differentiation in the root apical meristem. *Current Biology*, **25**, 3144–3150.
Knott, J.M., **Römer, P.** & **Sumper, M.** (2007) Putative spermine synthases from *Thalassiosira pseudonana* and *Arabidopsis thaliana* synthesize thermospermine rather than spermine. *FEBS Letters*, **581**, 3081–3086.
Koizumi, K., **Ookawa, T.**, **Satoh, H.** & **Hirasawa, T.** (2007) A wilty mutant of rice has impaired hydraulic conductance. *Plant & Cell Physiology*, **48**, 1219–1228.
Kooyers, N.J. (2015) The evolution of drought escape and avoidance in natural herbaceous populations. *Plant Science*, **234**, 155–162.
Laitinen, R.A.E. & **Nikoloski, Z.** (2022) Strategies to identify and dissect trade-offs in plants. *Molecular Ecology*, **33**, e16780. Available from: https://doi.org/10.1111/mec.16780
Le, Q.T., **Lee, W.J.**, **Choi, J.H.**, **Nguyen, D.T.**, **Truong, H.A.**, **Lee, S.A.** ***et al.*** (2022) The loss of function of the *NODULE INCEPTION-like PROTEIN 7* enhances salt stress tolerance in *Arabidopsis* seedlings. *Frontiers in Plant Science*, **12**, 743832.
Lens, F., **Gleason, S.M.**, **Bortolami, G.**, **Brodersen, C.**, **Delzon, S.** & **Jansen, S.** (2022) Functional xylem characteristics associated with drought-induced embolism in angiosperms. *The New Phytologist*, **236**, 2019–2036.
Li, X., **Yan, Z.**, **Zhang, M.**, **Wang, J.**, **Xin, P.**, **Cheng, S.** ***et al.*** (2023) SnoRNP is essential for thermospermine-mediated development in *Arabidopsis thaliana*. *Science China. Life Sciences*, **66**, 2–11.
Li, Z., **Hou, J.**, **Zhang, Y.**, **Zeng, W.**, **Cheng, B.**, **Hassan, M.J.** ***et al.*** (2020) Spermine regulates water balance associated with Ca^{2+}-dependent aquaporin (TrTIP2-1, TrTIP2-2 and TrPIP2-7) expression in plants under water stress. *Plant & Cell Physiology*, **61**, 1576–1589.
Liu, J.H., **Wang, W.**, **Wu, H.**, **Gong, X.** & **Moriguchi, T.** (2015) Polyamines function in stress tolerance: from synthesis to regulation. *Frontiers in Plant Science*, **6**, 827.
Lucas, W.J., **Groover, A.**, **Lichtenberger, R.**, **Furuta, K.**, **Yadav, S.R.**, **Helariutta, Y.** ***et al.*** (2013) The plant vascular system: evolution, development and functions. *Journal of Integrative Plant Biology*, **55**, 294–388.
Mai, H., **Qin, T.**, **Wei, H.**, **Yu, Z.**, **Pang, G.**, **Liang, Z.** ***et al.*** (2023) Overexpression of OsACL5 triggers environmentally-dependent leaf rolling and reduces grain size in rice. *Plant Biotechnology Journal*, **22**, 833–847. Available from: https://doi.org/10.1111/pbi.14227
Marina, M., **Sirera, F.V.**, **Rambla, J.L.**, **Gonzalez, M.E.**, **Blazquez, M.A.**, **Carbonell, J.** ***et al.*** (2013) Thermospermine catabolism increases *Arabidopsis thaliana* resistance to *Pseudomonas viridiflava*. *Journal of Experimental Botany*, **64**, 1393–1402.
Martignago, D., **Rico-Medina, A.**, **Blasco-Escámez, D.**, **Fontanet-Manzaneque, J.B.** & **Caño-Delgado, A.I.** (2020) Drought resistance by engineering plant tissue-specific responses. *Frontiers in Plant Science*, **10**, 1676.
Matsuo, H., **Fukushima, H.**, **Kurokawa, S.**, **Kawano, E.**, **Okamoto, T.**, **Motose, H.** ***et al.*** (2022) Loss of function of an Arabidopsis homologue of JMJD6 suppresses the dwarf phenotype of *acl5*, a mutant defective in thermospermine biosynthesis. *FEBS Letters*, **596**, 3005–3014.
Milhinhos, A., **Bollhöner, B.**, **Blazquez, M.A.**, **Novák, O.**, **Miguel, C.M.** & **Tuominen, H.** (2020) ACAULIS5 is required for cytokinin accumulation and function during secondary growth of *Populus* trees. *Frontiers in Plant Science*, **11**, 601858.
Milhinhos, A. & **Miguel, C.M.** (2013) Hormone interactions in xylem development: a matter of signals. *Plant Cell Reports*, **32**, 867–883.
Milhinhos, A., **Prestele, J.**, **Bollhöner, B.**, **Matos, A.**, **Vera-Sirera, F.**, **Rambla, J.L.** ***et al.*** (2013) Thermospermine levels are controlled by an auxin-dependent feedback loop mechanism in *Populus* xylem. *The Plant Journal*, **75**, 685–698.
Mo, H., **Wang, X.**, **Zhang, Y.**, **Yang, J.** & **Ma, Z.** (2015) Cotton ACAULIS5 is involved in stem elongation and the plant defense response to *Verticillium dahliae* through thermospermine alteration. *Plant Cell Reports*, **34**, 1975–1985.
Montesinos-Pereira, D., **Barrameda-Medina, Y.**, **Romero, L.**, **Ruiz, J.M.** & **Sánchez-Rodríguez, E.** (2014) Genotype differences in the metabolism of proline and polyamines under moderate drought in tomato plants. *Plant Biology (Stuttgart, Germany)*, **16**, 1050–1057.
Muñiz, L., **Minguet, E.G.**, **Singh, S.K.**, **Pesquet, E.**, **Vera-Sirera, F.**, **Moreau-Courtois, C.L.** ***et al.*** (2008) ACAULIS5 controls Arabidopsis xylem specification through the prevention of premature cell death. *Development*, **135**, 2573–2582.
Naka, Y., **Watanabe, K.**, **Sagor, G.H.M.**, **Niitsu, M.**, **Pillai, M.A.**, **Kusano, T.** ***et al.*** (2010) Quantitative analysis of plant polyamines including thermospermine during growth and salinity stress. *Plant Physiology and Biochemistry*, **48**, 527–533.
Nardini, A., **Gascò, A.**, **Trifilò, P.**, **Lo Gullo, M.A.** & **Salleo, S.** (2007) Ion-mediated enhancement of xylem hydraulic conductivity is not always suppressed by the presence of Ca^{2+} in the sap. *Journal of Experimental Botany*, **58**, 2609–2615.
Nekrasov, V., **Staskawicz, B.**, **Weigel, D.**, **Jones, J.D.** & **Kamoun, S.** (2013) Targeted mutagenesis in the model plant *Nicotiana benthamiana* using Cas9 RNA-guided endonuclease. *Nature Biotechnology*, **31**, 691–693.
Nir, I., **Shohat, H.**, **Panizel, I.**, **Olszewski, N.**, **Aharoni, A.** & **Weiss, D.** (2017) The tomato DELLA protein PROCERA acts in guard cells to promote stomatal closure. *Plant Cell*, **29**, 3186–3197.
Nishii, Y., **Koyama, D.**, **Fukushima, H.** & **Takahashi, T.** (2023) Suppression of the dwarf phenotype of an Arabidopsis mutant defective in thermospermine biosynthesis by a synonymous codon change in the SAC51 uORF. *Molecular Genetics and Genomics*, **298**, 1505–1514.
Pagliarani, C., **Casolo, V.**, **Ashofteh Beiragi, M.**, **Cavalletto, S.**, **Siciliano, I.**, **Schubert, A.** ***et al.*** (2019) Priming xylem for stress recovery depends on coordinated activity of sugar metabolic pathways and changes in xylem sap pH. *Plant, Cell & Environment*, **42**, 1775–1787.
Pál, M., **Tajti, J.**, **Szalai, G.**, **Peeva, V.**, **Végh, B.** & **Janda, T.** (2018) Interaction of polyamines, abscisic acid and proline under osmotic stress in the leaves of wheat plants. *Scientific Reports*, **8**, 12839.
Pan, R., **Geng, J.**, **Cai, J.** & **Tyree, M.T.** (2015) A comparison of two methods for measuring vessel length in woody plants. *Plant, Cell & Environment*, **38**, 2519–2526.
Petruzzellis, F., **Savi, T.**, **Bacaro, G.** & **Nardini, A.** (2019) A simplified framework for fast and reliable measurement of leaf turgor loss point. *Plant Physiology and Biochemistry*, **139**, 395–399.
Polticelli, F., **Basran, J.**, **Faso, C.**, **Cona, A.**, **Minervini, G.**, **Angelini, R.** ***et al.*** (2005) Lys300 plays a major role in the catalytic mechanism of maize polyamine oxidase. *Biochemistry*, **44**, 16108–16120.
Růžička, K., **Ursache, R.**, **Hejátko, J.** & **Helariutta, Y.** (2015) Xylem development - from the cradle to the grave. *The New Phytologist*, **207**, 519–535.
Sade, N., **Vinocur, B.J.**, **Diber, A.**, **Shatil, A.**, **Ronen, G.**, **Nissan, H.** ***et al.*** (2009) Improving plant stress tolerance and yield production: is the tonoplast aquaporin SlTIP2;2 a key to isohydric to anisohydric conversion? *The New Phytologist*, **181**, 651–661.
Sagor, G.H., **Takahashi, H.**, **Niitsu, M.**, **Takahashi, Y.**, **Berberich, T.** & **Kusano, T.** (2012) Exogenous thermospermine has an activity to induce a subset of the defense genes and restrict cucumber mosaic virus multiplication in *Arabidopsis thaliana*. *Plant Cell Reports*, **31**, 1227–1232.
Sagor, G.H., **Zhang, S.**, **Kojima, S.**, **Simm, S.**, **Berberich, T.** & **Kusano, T.** (2016) Reducing cytoplasmic polyamine oxidase activity in Arabidopsis increases salt and drought tolerance by reducing reactive oxygen species production and increasing defense gene expression. *Frontiers in Plant Science*, **7**, 214.
Salvi, D. & **Tavladoraki, P.** (2020) The tree of life of polyamine oxidases. *Scientific Reports*, **10**, 17858.
Sawchuk, M.G., **Edgar, A.** & **Scarpella, E.** (2013) Patterning of leaf vein networks by convergent auxin transport pathways. *PLoS Genetics*, **9**, e1003294.
Scholander, P.F., **Bradstreet, E.D.**, **Hemmingsen, E.A.** & **Hammel, H.T.** (1965) Sap pressure in vascular plants: negative hydrostatic pressure can be measured in plants. *Science*, **148**, 339–346.
Sharma, M. & **Pandey, G.K.** (2016) Expansion and function of repeat domain proteins during stress and development in plants. *Frontiers in Plant Science*, **6**, 1218.
Shinohara, S., **Okamoto, T.**, **Motose, H.** & **Takahashi, T.** (2019) Salt hypersensitivity is associated with excessive xylem development in a thermospermine-deficient mutant of *Arabidopsis thaliana*. *The Plant Journal*, **100**, 374–383.
Solé-Gil, A., **Hernández-García, J.**, **López-Gresa, M.P.**, **Blázquez, M.A.** & **Agustí, J.** (2019) Conservation of thermospermine synthase activity in vascular and non-vascular plants. *Frontiers in Plant Science*, **10**, 663.
Sperry, J.S. (2003) Evolution of water transport and xylem structure. *International Journal of Plant Sciences*, **164**, 115–127.
Takano, A., **Kakehi, J.** & **Takahashi, T.** (2012) Thermospermine is not a minor polyamine in the plant kingdom. *Plant & Cell Physiology*, **53**, 606–616.

Tavladoraki, P., **Cona, A.** & **Angelini, R.** (2016) Copper-containing amine oxidases and FAD-dependent polyamine oxidases are key players in plant tissue differentiation and organ development. *Frontiers in Plant Science*, **7**, 824.

Tavladoraki, P., **Rossi, M.N.**, **Saccuti, G.**, **Perez-Amador, M.A.**, **Polticelli, F.**, **Angelini, R.** ***et al.*** (2006) Heterologous expression and biochemical characterization of a polyamine oxidase from Arabidopsis involved in polyamine back conversion. *Plant Physiology*, **141**, 1519–1532.

Tavladoraki, P., **Schininà, M.E.**, **Cecconi, F.**, **Di Agostino, S.**, **Manera, F.**, **Rea, G.** ***et al.*** (1998) Maize polyamine oxidase: primary structure from protein and cDNA sequencing. *FEBS Letters*, **426**, 62–66.

Tiburcio, A.F., **Altabella, T.**, **Bitrián, M.** & **Alcázar, R.** (2014) The roles of polyamines during the lifespan of plants: from development to stress. *Planta*, **240**, 1–18.

Tisi, A., **Federico, R.**, **Moreno, S.**, **Lucretti, S.**, **Moschou, P.N.**, **Roubelakis-Angelakis, K.A.** ***et al.*** (2011) Perturbation of polyamine catabolism can strongly affect root development and xylem differentiation. *Plant Physiology*, **157**, 200–215.

Tomasella, M., **Casolo, V.**, **Aichner, N.**, **Petruzzellis, F.**, **Savi, T.**, **Trifilò, P.** ***et al.*** (2019) Non-structural carbohydrate and hydraulic dynamics during drought and recovery in *Fraxinus ornus* and *Ostrya carpinifolia* saplings. *Plant Physiology and Biochemistry*, **145**, 1–9.

Tong, W., **Yoshimoto, K.**, **Kakehi, J.**, **Motose, H.**, **Niitsu, M.** & **Takahashi, T.** (2014) Thermospermine modulates expression of auxin-related genes in Arabidopsis. *Frontiers in Plant Science*, **5**, 94.

Torres-Ruiz, J.M., **Jansen, S.**, **Choat, B.**, **McElrone, A.J.**, **Cochard, H.**, **Brodribb, T.J.** ***et al.*** (2015) Direct X-ray microtomography observation confirms the induction of embolism upon xylem cutting under tension. *Plant Physiology*, **167**, 40–43.

Tyree, M.T. & **Ewers, F.W.** (1991) The hydraulic architecture of trees and other woody plants. *The New Phytologist*, **119**, 345–360.

Upadhyay, R.K., **Fatima, T.**, **Handa, A.K.** & **Mattoo, A.K.** (2021) Differential association of free, conjugated, and bound forms of polyamines and transcript abundance of their biosynthetic and catabolic genes during drought/salinity stress in tomato (*Solanum lycopersicum* L.) leaves. *Frontiers in Plant Science*, **12**, 743568.

Van Eck, J., **Keen, P.** & **Tjahjadi, M.** (2019) *Agrobacterium tumefaciens*-mediated transformation of tomato. *Methods in Molecular Biology*, **1864**, 225–234.

van Roekel, J.S., **Damm, B.**, **Melchers, L.S.** & **Hoekema, A.** (1993) Factors influencing transformation frequency of tomato (*Lycopersicon esculentum*). *Plant Cell Reports*, **12**, 644–647.

Venturas, M.D., **Sperry, J.S.** & **Hacke, U.G.** (2017) Plant xylem hydraulics: what we understand, current research, and future challenges. *Journal of Integrative Plant Biology*, **59**, 356–389.

Vera-Sirera, F., **De Rybel, B.**, **Úrbez, C.**, **Kouklas, E.**, **Pesquera, M.**, **Álvarez-Mahecha, J.C.** ***et al.*** (2015) A bHLH-based feedback loop restricts vascular cell proliferation in plants. *Developmental Cell*, **35**, 432–443.

Vera-Sirera, F., **Minguet, E.G.**, **Singh, S.K.**, **Ljung, K.**, **Tuominen, H.**, **Blázquez, M.A.** ***et al.*** (2010) Role of polyamines in plant vascular development. *Plant Physiology and Biochemistry*, **48**, 534–539.

Verna, C., **Sawchuk, M.G.**, **Linh, N.M.** & **Scarpella, E.** (2015) Control of vein network topology by auxin transport. *BMC Biology*, **13**, 94.

Verslues, P.E. & **Sharma, S.** (2010) Proline metabolism and its implications for plant-environment interaction. *Arabidopsis Book*, **8**, e0140.

Vujcic, S., **Liang, P.**, **Diegelman, P.**, **Kramer, D.L.** & **Porter, C.W.** (2003) Genomic identification and biochemical characterization of the mammalian polyamine oxidase involved in polyamine back-conversion. *The Biochemical Journal*, **370**, 19–28.

Wang, R., **Zhang, L.**, **Zhang, S.**, **Cai, J.** & **Tyree, M.T.** (2014) Water relations of *Robinia pseudoacacia* L.: do vessels cavitate and refill diurnally or are R-shaped curves invalid in Robinia? *Plant, Cell & Environment*, **37**, 2667–2678.

Wang, W. & **Liu, J.H.** (2016) CsPAO4 of *Citrus sinensis* functions in polyamine terminal catabolism and inhibits plant growth under salt stress. *Scientific Reports*, **6**, 31384.

Wang, W., **Peng, Z.** & **Yang, J.** (2022) Single-sequence protein structure prediction using supervised transformer protein language models. *Nature Computational Science*, **2**, 804–814.

Wang, W., **Shi, S.**, **Kang, W.** & **He, L.** (2023) Enriched endogenous free Spd and Spm in alfalfa (*Medicago sativa* L.) under **drought stress** enhance **drought** tolerance by inhibiting H(2)O(2) production to increase antioxidant enzyme activity. *Journal of Plant Physiology*, **291**, 154139.

Weber, E., **Engler, C.**, **Gruetzner, R.**, **Werner, S.** & **Marillonnet, S.** (2011) A modular cloning system for standardized assembly of multigene constructs. *PLoS One*, **6**, e16765.

Wroblewski, T., **Tomczak, A.** & **Michelmore, R.** (2005) Optimization of agrobacterium-mediated transient assays of gene expression in lettuce, tomato and Arabidopsis. *Plant Biotechnology Journal*, **3**, 259–273.

Xie, K., **Minkenberg, B.** & **Yang, Y.** (2015) Boosting CRISPR/Cas9 multiplex editing capability with the endogenous tRNA-processing system. *Proceedings of the National Academy of Sciences of the United States of America*, **112**, 3570–3575.

Yamaguchi, S. (2008) Gibberellin metabolism and its regulation. *Annual Review of Plant Biology*, **59**, 225–251.

Yoshimoto, K., **Noutoshi, Y.**, **Hayashi, K.**, **Shirasu, K.**, **Takahashi, T.** & **Motose, H.** (2012a) A chemical biology approach reveals an opposite action between thermospermine and auxin in xylem development in Arabidopsis thaliana. *Plant & Cell Physiology*, **53**, 635–645.

Yoshimoto, K., **Noutoshi, Y.**, **Hayashi, K.**, **Shirasu, K.**, **Takahashi, T.** & **Motose, H.** (2012b) Thermospermine suppresses auxin-inducible xylem differentiation in *Arabidopsis thaliana*. *Plant Signaling & Behavior*, **7**, 937–939.

Zarza, X., **Atanasov, K.**, **Marco, F.**, **Arbona, V.**, **Carrasco, P.**, **Kopka, J.** ***et al.*** (2017) Polyamine oxidase 5 loss-of-function mutations in *Arabidopsis thaliana* trigger metabolic and transcriptional reprogramming and promote salt stress tolerance. *Plant, Cell & Environment*, **40**, 527–542.

Zhang, J., **Zhang, H.**, **Srivastava, A.K.**, **Pan, Y.**, **Bai, J.**, **Fang, J.** ***et al.*** (2018) Knockdown of rice microRNA166 confers drought resistance by causing leaf rolling and altering stem xylem development. *Plant Physiology*, **176**, 2082–2094.

Zhu, L., **Qian, N.**, **Sun, Y.**, **Lu, X.**, **Duan, H.** & **Qian, L.** (2021) *Pseudomonas fluorescens* DN16 enhances cucumber defense responses against the necrotrophic pathogen *Botrytis cinerea* by regulating thermospermine catabolism. *Frontiers in Plant Science*, **12**, 645338.